

FINAL REPORT

Shallow Water Lidar for Target Morphology: Impacts of Surface
Roughness and Turbidity

SERDP Project MR18-1459

NOVEMBER 2019

Jeffrey Thayer
Atmospheric & Space Technology Research
Associates, LLC (ASTRA)

Distribution Statement A

This document has been cleared for public release



Page Intentionally Left Blank

This report was prepared under contract to the Department of Defense Strategic Environmental Research and Development Program (SERDP). The publication of this report does not indicate endorsement by the Department of Defense, nor should the contents be construed as reflecting the official policy or position of the Department of Defense. Reference herein to any specific commercial product, process, or service by trade name, trademark, manufacturer, or otherwise, does not necessarily constitute or imply its endorsement, recommendation, or favoring by the Department of Defense.

Page Intentionally Left Blank

REPORT DOCUMENTATION PAGE

*Form Approved
OMB No. 0704-0188*

The public reporting burden for this collection of information is estimated to average 1 hour per response, including the time for reviewing instructions, searching existing data sources, gathering and maintaining the data needed, and completing and reviewing the collection of information. Send comments regarding this burden estimate or any other aspect of this collection of information, including suggestions for reducing the burden, to Department of Defense, Washington Headquarters Services, Directorate for Information Operations and Reports (0704-0188), 1215 Jefferson Davis Highway, Suite 1204, Arlington, VA 22202-4302. Respondents should be aware that notwithstanding any other provision of law, no person shall be subject to any penalty for failing to comply with a collection of information if it does not display a currently valid OMB control number.
PLEASE DO NOT RETURN YOUR FORM TO THE ABOVE ADDRESS.

1. REPORT DATE (DD-MM-YYYY) 11/11/2019	2. REPORT TYPE SERDP Final Report	3. DATES COVERED (From - To) 3/13/2018 - 9/13/2019
--	---	--

4. TITLE AND SUBTITLE Shallow Water Lidar for Target Morphology: Impacts of Surface Roughness and Turbidity	5a. CONTRACT NUMBER 18-C-0026
	5b. GRANT NUMBER
	5c. PROGRAM ELEMENT NUMBER

6. AUTHOR(S) Jeffrey P. Thayer	5d. PROJECT NUMBER MR18-1459
	5e. TASK NUMBER
	5f. WORK UNIT NUMBER

7. PERFORMING ORGANIZATION NAME(S) AND ADDRESS(ES) Atmospheric & Space Technology Research Associates 5777 Central Avenue, Suite 221 Boulder, CO 80301	8. PERFORMING ORGANIZATION REPORT NUMBER MR18-1459
--	--

9. SPONSORING/MONITORING AGENCY NAME(S) AND ADDRESS(ES) Strategic Environmental Research and Development Program 4800 Mark Center Drive, Suite 17D03 Alexandria, VA 22350-3605	10. SPONSOR/MONITOR'S ACRONYM(S) SERDP
	11. SPONSOR/MONITOR'S REPORT NUMBER(S) MR18-1459

12. DISTRIBUTION/AVAILABILITY STATEMENT
DISTRIBUTION STATEMENT A. Approved for public release: distribution unlimited.

13. SUPPLEMENTARY NOTES

14. ABSTRACT
The problem is to detect, classify, and remediate military munitions found in aquatic environments such as ponds, lakes, rivers, estuaries, and coastal and open ocean areas. A specific need is for technology to solve this problem with munitions residing in depths less than five meters. This shallow-water domain includes an assortment of unexploded ordnance that are the most likely to be encountered by the public and are expected to experience the most mobility. Many sensor technologies designed to detect, classify, and remediate munitions are challenged by this unique environment and suffer in performance, access, navigation, deployment, viewing, sensor standoff distance, and damage by changing bottom topography or obstructions. The project objective is to investigate how water conditions (i.e. wavy surfaces and turbid water columns) might impact the feasibility of using a new above-water lidar technology for the classification of the aquatic environment and the identification of munitions in waters less than five meters deep with vertical and horizontal resolutions at centimeter levels. The SEED-funded activity studied the interactions of pulsed laser light with wavy water surfaces and turbid water columns and their effect on the lidar's 3-D mapping capability.

15. SUBJECT TERMS
LiDAR, littoral zone, munitions, morphology, turbidity, waves, shallow waters, laser propagation

16. SECURITY CLASSIFICATION OF:			17. LIMITATION OF ABSTRACT	18. NUMBER OF PAGES	19a. NAME OF RESPONSIBLE PERSON
a. REPORT	b. ABSTRACT	c. THIS PAGE			Jeffrey P. Thayer
UNCLASS	UNCLASS	UNCLASS	UNCLASS	52	19b. TELEPHONE NUMBER (Include area code) 720-545-3050

Page Intentionally Left Blank

Table of Contents

List of Tables	ii
List of Figures	ii
List of Acronyms	iii
Keywords	iii
Acknowledgements	iii
Abstract	1
Introduction and Objectives	1
Technical Approach	2
Results	2
Benefits	2
Executive Summary	3
Introduction	3
Objectives	3
Technical Approach	4
Results and Discussion	4
Implications for Future Research and Benefits	12
Objective	15
Background	15
Materials and Methods	18
Results and Discussion	25
Conclusions and Implications for Future Research	40
Literature Cited	43

List of Tables

Table 1. Calibrated Particles

List of Figures

- Figure E1.* Lidar scan of submerged brick in 26 cm of water
Figure E2. Comparison between modeled lidar ranges
Figure E3. Graph showing results for the full wave test set
Figure E4. Lidar MCLST simulation
Figure E5. Bottom return signal voltage as a function of particle concentration
Figure E6. Drone-based, scanning topo/bathy lidar measurements
Figure E7. Drone-based scanning topo/bathy lidar flying over a lagoon with a coral bed
Figure E8. Lidar maximum depth performance in meters
Figure E9. Outdoor experiments under wavy surface conditions
Figure 1. Lidar measurements dependent on Fermat's principle of least time
Figure 2. Combined surface wave spectrum (2D JONSWAP)
Figure 3. Simulated lidar beamlets time of flight distribution
Figure 4. MCLST simulation of optical depth penetration
Figure 5. Image of the lidar-turbidity test setup
Figure 6. Design of a small wave tank
Figure 7. Lidar scan of submerged brick in 26 cm of water
Figure 8. Graph showing many of the results for the full wave test set
Figure 9. Scatter plot of all wave tests colored by discrepancy between the actual test and the lidar model
Figure 10. Comparison between modeled lidar range distribution and experimentally measured lidar range distribution
Figure 11. Lidar MCLST simulation of spreading lidar beam propagating through the water column with a uniform distribution of 10 nm spherical particles
Figure 12. Lidar MCLST simulation of spreading of a lidar beam propagating through the water column with a uniform distribution of 10 nm spherical particles.
Figure 13. Lidar MCLST simulation of the extinction coefficient versus wavelength for different particle sizes
Figure 14. Lidar MCLST simulation of the normalized scattering phase function at 532 nm for different particle sizes
Figure 15. Bottom return signal voltage as a function of particle concentration for four discrete particle sizes
Figure 16. Drone-based, scanning topo/bathy lidar measurements over a shoreline
Figure 17. Drone-based scanning topo/bathy lidar flying over a lagoon with a coral bed
Figure 18. Lidar maximum depth performance in meters with turbidity levels in nephelometer turbidity units (NTU)
Figure 19. Outdoor experiments under wavy surface conditions off the coast of Oahu

List of Acronyms

ALB – Airborne Lidar Bathymetry
ASTRA – Atmospheric & Space Technology Research Associates LLC
ASTRALiTe - ASTRA Lidar Technologies
AUV – Automated Underwater Vehicle
CU – University of Colorado
DoD – Department of Defense
DVL – Doppler Velocity Log
EMI – Electromagnetic Induction
GPS – Global Positioning System
IMU – Inertial Measurement Unit
lidar – Light Detection and Ranging
LLSS – Laser Line Scanning Sensors
LBL – Long Base Line
MCLST – Monte Carlo Lidar Simulation Tool
MR – Munitions Response
NTU – Nephelometer Turbidity Units
ROV – Remotely Operated Vehicle
RTK-GPS – Real Time Kinematic Global Positioning System
SEED – SERDP Exploratory Development
SERDP – Strategic Environmental Research and Development Program
SfM – Structure from Motion
SON – Statement of Need
ToF – Time of Flight
UAS – Unmanned Aerial System
USBL – Ultrashort Baseline
UXO – Underwater Unexploded Ordnance

Keywords

LiDAR, littoral zone, munitions, morphology, turbidity, waves, shallow waters, laser propagation

Acknowledgements

The ASTRALiTe team would like to thank the support from Dr. Herb Nelson in providing guidance and feedback on our project. Sarah Barlow has also been of great help. The project has also benefited from the support by the ASTRA team whose efforts and dedication made many of the flight opportunities possible. The Applied Research Lab at the University of Hawaii and the State of Colorado also provided support which benefited the results of this project.

Abstract

Introduction and Objectives. The problem is to detect, classify, and remediate military munitions found in aquatic environments such as ponds, lakes, rivers, estuaries, and coastal and open ocean areas. A specific need is for technology to solve this problem with munitions residing in depths less than five meters. This shallow-water domain includes an assortment of unexploded ordnance that are the most likely to be encountered by the public and are expected to experience the most mobility. Many sensor technologies designed to detect, classify, and remediate munitions are challenged by this unique environment and suffer in performance, access, navigation, deployment, viewing, sensor standoff distance, and damage by changing bottom topography or obstructions.

The project objective is to investigate how water conditions (i.e. wavy surfaces and turbid water columns) might impact the feasibility of using a new above-water lidar technology for the classification of the aquatic environment and the identification of munitions in waters less than five meters deep with vertical and horizontal resolutions at centimeter levels. The SEED-funded activity studied the interactions of pulsed laser light with wavy water surfaces and turbid water columns and their effect on the lidar's 3-D mapping capability.

Technical Approach. The technical approach used a variety of materials and methods involving numerical simulation, controlled lab experimentation, instrument prototyping, and outdoor experiments. Simulations included a Monte Carlo scheme that followed photons as they propagated through turbid media and a ray trace scheme to map the effects of surface reflection, transmission, and refraction due to wavy surfaces. Indoor experiments were carried out using the lidar technique with a graduated cylinder and a water tank to determine turbidity and surface wave effects on lidar measurements. A prototype drone-based, scanning topographic/bathymetric lidar system was also used to demonstrate outdoor capabilities.

Results. Wave properties were simulated and experimentally generated to evaluate the lidar detection of underwater objects. Variable refraction due to changing wave slope and time delay due to changing wave amplitude were the dominant factors in producing variability in lidar range and cross-range measurements. In turbid waters, both particle size and particle concentration matter when considering the lidar depth performance. Larger particles, relative to the excitation wavelength, proved less detrimental to lidar detections than smaller particles due to their preferential forward scatter. Outdoor drone-flight experiments demonstrated the potential capability of this technology to detect underwater munitions in shallow waters (< 5 m) with a total empirical precision estimate of < 10 cm (lidar error <1 cm, platform error < 5cm, water conditions error < 5 cm). These lidar measurements experienced both wavy and turbid conditions and provided empirical evidence for the technique's ability to operate in environments relevant to munitions response.

Benefits. This research is of great interest to the Department of Defense (DoD) and scientific communities due to its ability to observe at high resolution a wide variety of shallow-water aquatic environments that have been, up to now, were inaccessible due to limited technologies. The results further address DoD needs by establishing a new technology with the ability to detect, range, and classify underwater objects with high vertical and horizontal resolution without making contact with the water. This lidar capability can be highly complementary to other SERDP techniques.

Executive Summary

Introduction

As described in the Statement of Need (SON) in the Munitions Response (MR) program area, MRSEED-18-S1: Detection, Classification, and Remediation of Military Munitions Underwater, the problem to be addressed is to develop technologies to detect, classify, and remediate military munitions found in aquatic environments. A specific need is for technology to operate in depths less than 5 meters: where munitions of interest may be found in a wide variety of aquatic environments, such as ponds, lakes, rivers, estuaries, and coastal areas; where munitions are likely to be encountered by the public; and where mobility of munitions is expected to be an issue. Target morphometry (the ability to accurately determine the dimensions - length, width, and height of targets identified compared to the known dimensions of these same targets) and target positioning (the ability to accurately determine the specific location of targets) are primary methods for reacquisition and remediation of underwater unexploded ordnances (UXOs). Sensors considered previously for addressing this need include electromagnetic induction (EMI), magnetic, optical, sonar/acoustic, chemical sensors, and laser line scanning sensors (LLSS). Platforms include autonomous underwater vehicles (AUVs), remotely operated vehicles (ROVs), and towed arrays. Navigation and positioning technologies include long base line (LBL), ultrashort baseline (USBL), Doppler velocity log (DVL), real-time kinematic global positioning system (RTK-GPS), and inertial navigation technologies.

Many acoustic systems, such as high-frequency towed or hull-mounted side scan or multi-beam sonar systems, do not perform optimally in water depths shallower than 5 meters where issues associated with multipath, narrow beam widths, navigation and positioning with waves, and currents limit performance. In these shallow depths magnetic and EMI systems that crawl, or are towed across the bottom, are employed but their effectiveness is limited in resolution, noise contamination, and operations. Optical systems producing 2-D imagery have been demonstrated, as have LLSS. **However, these systems, along with the others, require submergence in water, and these shallow regimes create unique challenges in access, navigation, deployment, viewing, and sensor standoff distance. Furthermore, changing bottom topography or obstructions pose a risk to equipment and personnel in this dynamic shallow-water environment.** Thus new technologies need to be explored to adequately address this challenging problem and likely the solution will need to operate out of the water.

An above-water lidar system is the proposed solution and this SEED project is to investigate the practicability of applying such a technique under conditions of wavy surfaces and turbid water.

Objectives

The main objective of the SEED research effort is to investigate the effects of water surface roughness and turbidity on the performance of an above-water lidar technique in detecting and classifying underwater objects in shallow waters (< 5 meters). The technical objectives of the SEED grant are specified by the following tasks/criteria in the order they were carried out. These deviate slightly from the original task list to better organize activities and results in this report.

Task 1) Incorporate Water Surface Roughness into Lidar Models: This task required advancing lidar simulations to evaluate theoretically how surface waves will effect lidar performance.

Task 2) Incorporate Water Turbidity into Lidar Models: This task required advancing lidar simulations to evaluate theoretically how water turbidity will effect lidar performance.

Task 3) Measure Effect of Turbidity: This task required a controlled lidar experiment of depth measurements while introducing known properties of suspended particulates to evaluate optical propagation through particles of known size and concentration.

Task 4) Measure Effect of Waviness of Water Surface: This task required the construction of a small wave tank and lidar detection system to perform controlled indoor experiments that illuminate the effects of wave amplitude and frequency on the lidar's accuracy and precision in describing underwater objects.

Task 5) Outdoor Environmental Test: This task required the deployment of a prototype lidar system over water bodies of various conditions to demonstrate outdoor capabilities.

Technical Approach

The technical approach used a variety of materials and methods involving simulation, controlled lab experimentation, instrument prototyping, and outdoor experiments. Simulations included a Monte Carlo scheme that followed photons as they propagated through turbid media and a ray trace scheme to map the effects of surface reflection, transmission, and refraction due to wavy surfaces. Indoor experiments were carried out using the lidar technique with a graduated cylinder and a water tank to determine turbidity and surface wave effects on lidar measurements. A prototype drone-based, scanning topographic/bathymetric lidar system was also used to demonstrate outdoor capabilities.

Results and Discussion

The results of the numerical and experimental activities are combined to explain the effects of surface waves and turbidity on lidar performance. Surface wave effects are summarized by findings related to the surface wave-lidar model and wave tank experiments. These findings are listed below using the identifier "W#" to indicate a water-surface findings. Turbidity effects are summarized by findings related to Monte Carlo modeling and suspended-particle lab experiments. These findings use the identifier "T#". Outdoor experiments are presented that demonstrate the potential capability of this technology to detect underwater munitions in shallow waters (< 5 m). These measurements experienced both wavy and turbid conditions and provide empirical evidence for the technique's ability to operate in environments relevant to munitions response. These are identified using "O#".

Surface wave effects

Finding #1 (W1): A surface wave-lidar model was developed to assess the influence of waves on the lidar's ability to determine the dimensions of an underwater object. The model incorporates a realistic ocean surface-wave model with a lidar ray-trace scheme that simulates

the lidar beam interaction with a wavy surface. The model has flexibility to produce a range of wavy surfaces and lidar parameters.

Finding #2 (W2): A wave tank was built and combined with a nadir-viewing lidar to observe the effects of wavy surfaces on the actual retrieval of range information from the backscattered lidar returns. The wave tank has flexibility to generate a range of wavelengths, from 0.12 to 0.7 meters, and amplitudes up to 4 centimeters. These waves can be simulated by the surface-wave model.

Finding #3 (W3): A lidar target morphometry test of a submerged brick using the wave tank at a specific wavelength and amplitude illustrated a spread in range values and cross-range values due to surface waves that blurred the edge, spread the top, and introduced a slight bias towards longer ranges – See Figure E1. These effects were replicated by the wave model and identified that refraction through the wave slope (ratio of wave amplitude to wavelength) was impacting the cross-range error the most, while the changing water path length due the crest and the valley of the wave caused the spread in range estimates. The range bias to longer range is attributed to refraction where a nadir viewing lidar will always increase in range when experiencing a slope other than flat. These results will vary depending on the wave representation and particularly on the ratio of amplitude to wavelength.

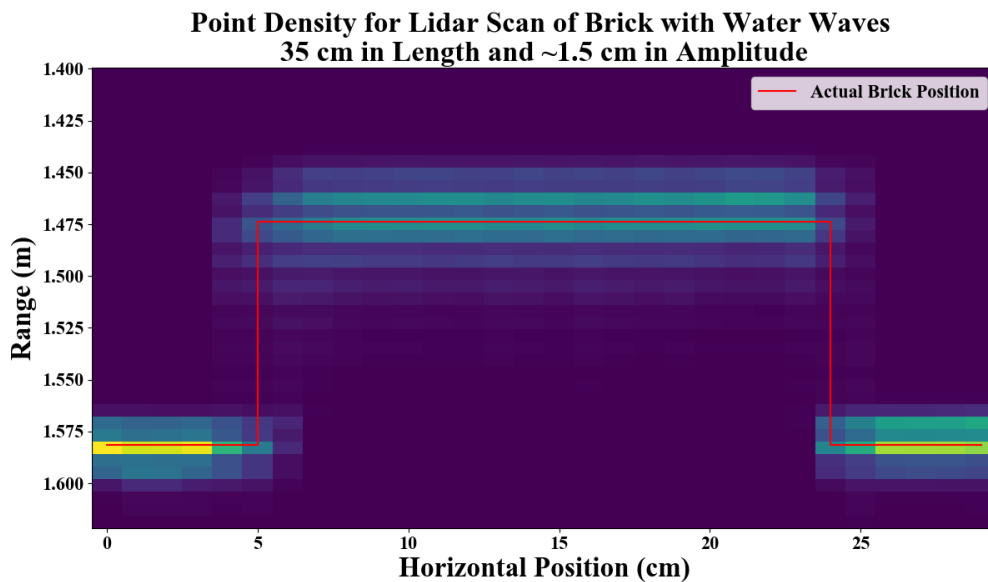


Figure E1. Lidar scan of submerged brick in 26 centimeters of water. The number of detections with range is displayed using a normalized color mapping. The actual brick shape is also shown for reference in red.

Finding #4 (W4): The absolute estimate of range errors for all wave conditions is highly dependent on the lidar parameters and the water surface wave properties. The effects of refraction due to changing wave slope and time delay due to wave amplitude changes are clearly the dominant factors in producing variability in range and cross range directions. The effects are observed in the data and captured by the wave-lidar model – see Figure E2. Specific conditions will need to be known to fully quantify the effects but a conservative uncertainty of several centimeters (< 5 cm) in shallow waters (< 5m) is the expected effect of surface waves on lidar target morphometry.

Lidar Range Distribution for 30 cm Waves with ~1 cm Amplitude

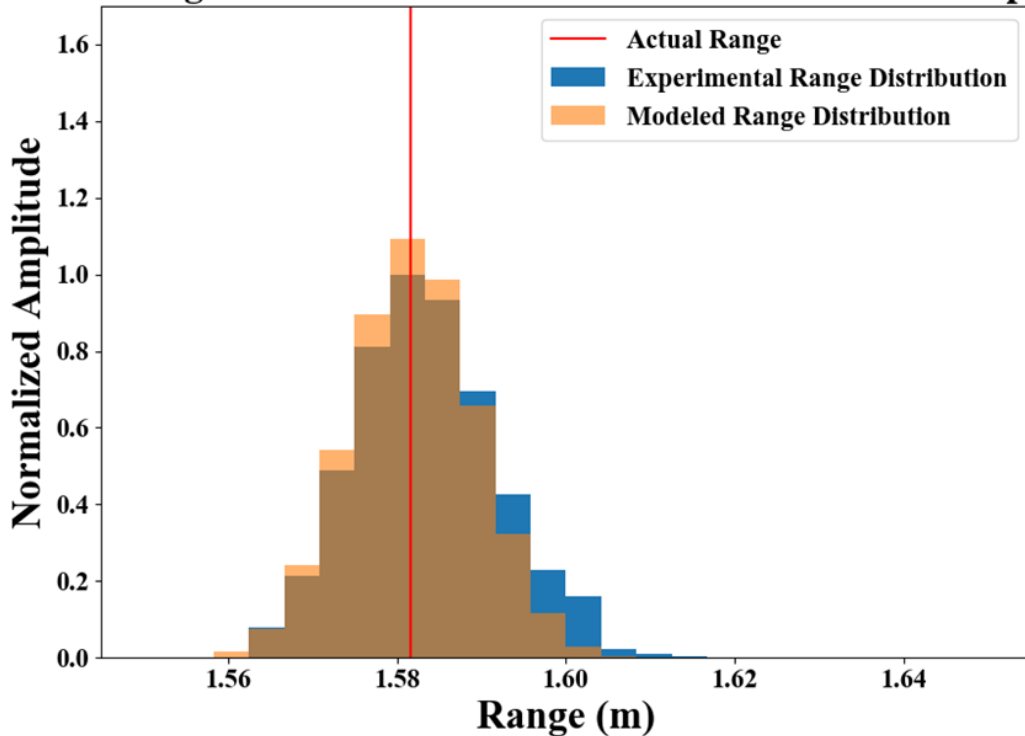


Figure E2. Comparison between modeled lidar range distribution and experimentally measured lidar range distribution for lidar aimed at tank bottom with 30 cm waves at ~1 cm amplitude.

Finding #5 (W5): Through a series of wave tank experiments with varied wavelengths and amplitudes (22 different tests), the surface wave-lidar model was validated and can serve as a useful tool to evaluate lidar performance and help optimally design lidar parameters given an actual ocean wave spectrum – see Figure E3.

Lidar-Wave Test Bottom Measurement Results

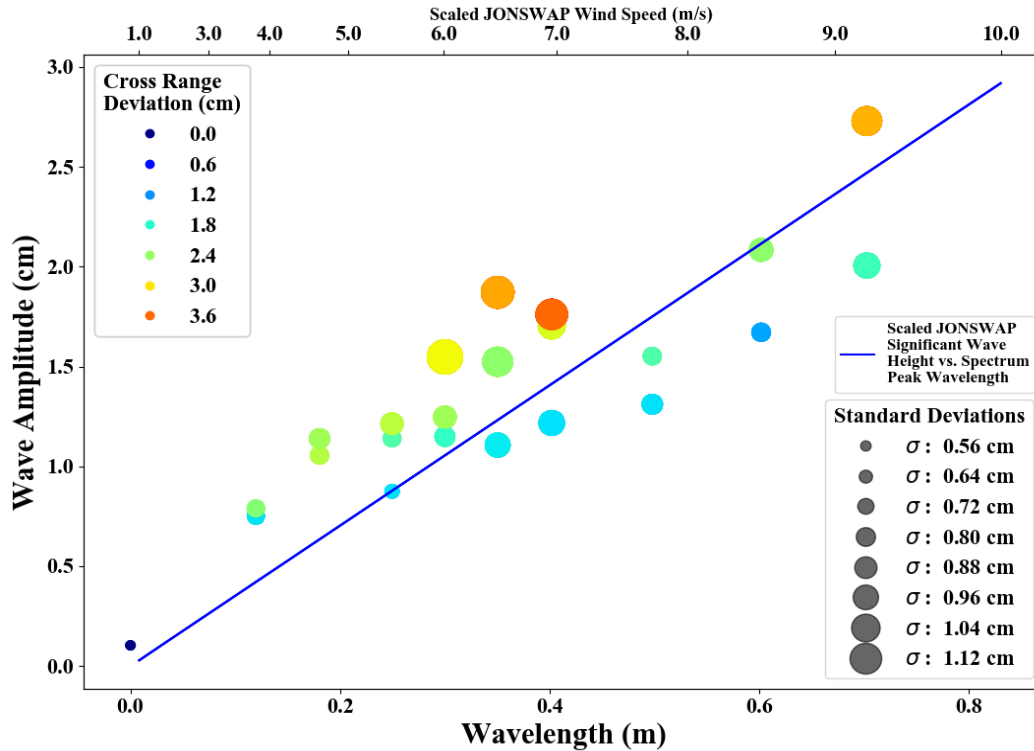


Figure E3. Graph showing many of the results for 22 different wave tests of different wavelength and amplitude. Each scatter plot point is its own wavelength and amplitude. The size of each point refers to its increase in standard deviation from a still water distribution. The color of each point represents the horizontal deviation caused by the waves. The JONSWAP significant wave height and peak spectral wavelength are also plotted with the scaling factor of 70 applied. The wind speed that corresponds to each JONSWAP peak wavelength is also shown at the top of the plot.

Turbidity effects

Finding #6 (T1): A 3-D Monte Carlo model, the ASTRALiTe Monte Carlo Lidar Simulation Tool (MCLST), was developed to simulate laser light propagation through turbid water. Various lidar (beam size, divergence, polarization state, wavelength) and environmental (particulate size, particle density, index of refraction, absorption) variables can be adjusted in the model to fully explore the trade space of lidar parameters and environmental conditions. In the simulations photons from the lidar laser pulse are propagated through the water medium with uniformly distributed particulates of different particle size relative to the laser wavelength and each photon is tracked and counted to understand how the suspended particulate matter effects the laser light.

Finding #7 (T2): An experimental setup was built to validate the turbidity propagation model by mounting a stationary lidar system over a graduated cylinder and carefully controlling turbidity levels for specific particle sizes.

Finding #8 (T3): Experiments were conducted to match the model's conditions as closely as possible. A calibrated quantity of particles of uniform size and material are incrementally introduced into pure water and thoroughly mixed. Five different particle sizes were tested whose

scattering regime ranged from Rayleigh-Mie-Geometric scattering. For verification, the water turbidity was measured by a Nephelometer and recorded in Nephelometer Turbidity Units (NTUs).

Finding #9 (T4): The model simulations illustrated the adverse effect of beam spreading caused by the presence of suspended particulates. Using the size parameter as a reference, the spreading of the beam was greater for particles with size parameters closer to one (i.e., small particles-weakly Mie scattering) than for size parameters closer to one hundred (i.e., larger particles-Geometric scattering). These particulate scattering aspects will affect the ability to detect and classify objects, as a spreading beam will make small objects more difficult to discern and, for a given lidar receiver field-of-view, the number of photons received for detection will be reduced as many photons are scattered out of the path before returning to the lidar.

Finding #10 (T5): Congruently, the depth penetration was found to be size-parameter dependent with larger particles allowing for greater depth penetration than the smaller particles. The model showed, through simulations of the scattering phase function, that the larger particles produced much more forward scattering keeping the photons in line with the lidar receiver field of view – see Figure E4. This benefits detections to deeper waters than if the water column was populated with smaller particles of equal concentration.

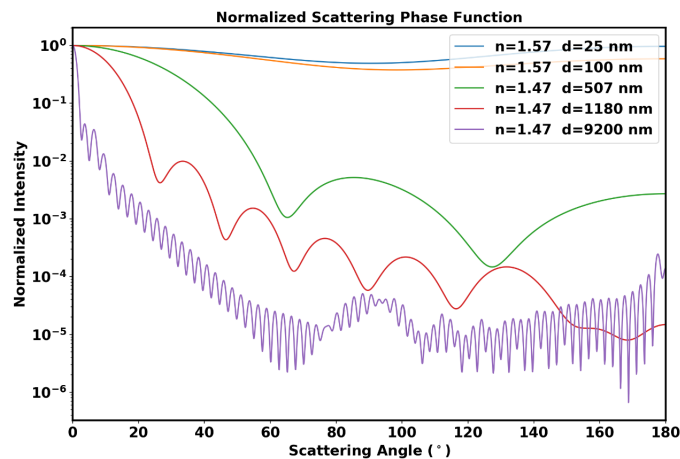


Figure E4. Lidar MCLST simulation of the normalized scattering phase function at 0.532 micron for different particle sizes used in the lab experiments.

Finding #11 (T6): Empirical results from the turbidity experimental setup confirmed the findings of the model with larger particles causing less light loss than the smaller particles for the same concentration. However, the outcomes can be less intuitive when the size parameter lies between weak and strong Mie scattering regimes. As simulated, the scattering efficiency and scattering phase function are important parameters for determining laser light propagation and these depend on size parameter, particle index of refraction, particle concentrations and related optical properties. These properties will play an important role when working with particles in

between weak and strong Mie scattering regimes (essentially between 0.01 and 1 micron particles when illuminated by 0.532 micron light) – see Figure E5.

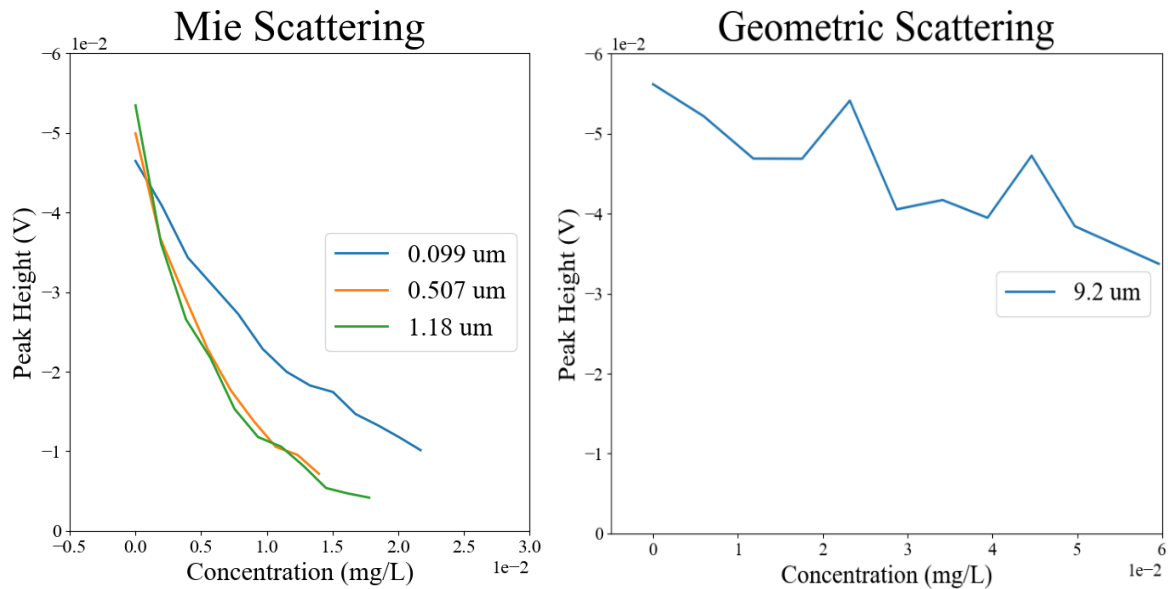


Figure E5. Bottom return signal voltage as a function of particle concentration for four discrete particle sizes. Sizes demonstrate the scattering regimes of weak and strong Mie scattering models and Geometric scattering. Note the horizontal range of the concentration for Geometric Scattering is extended to 0.060 mg/L.

Finding #12 (T7): The lidar’s optical detection of signals from underwater objects is favored by forward scattering of light caused by larger suspended particulates. These photons will remain in the lidar’s field of view and contribute to the population of photons scattered back to the lidar receiver by the object. Thus, particle size and particle concentration matter when considering the lidar depth performance. A Nephelometer measures extinction at a given wavelength at a 90-degree scattering angle and thus does not capture all aspects of how lidar is influenced by turbidity. However, the straight forward Nephelometer measurement serves as a common reference by which to relate lidar depth performance in different water bodies (as will be demonstrated in the outdoor experiments).

Outdoor results with both turbidity and waves

Outdoor experiments were carried out using a prototype drone-based, scanning lidar system in several different environments.

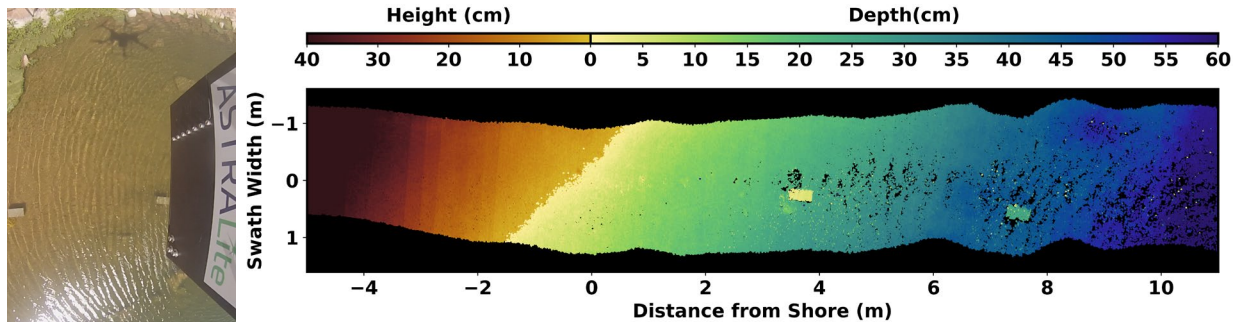


Figure E6. Drone-based, scanning topo/bathy lidar measurements over a shoreline with two cinder blocks submerged in the water.

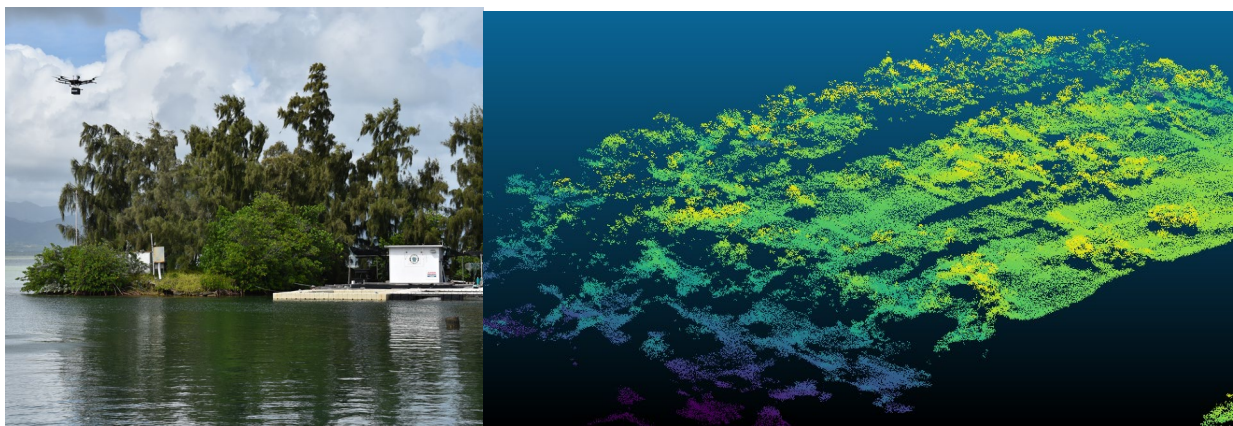


Figure E7. Drone-based scanning topo/bathy lidar flying over a lagoon with a coral bed (left). The resultant 3-D point cloud of the coral bed displaying great detail with the color variation indicating depth from water surface (yellow is about 1 meter depth and dark blue is about 4 meter depth)

Finding #13 (O1): Outdoor experiments with a prototype drone-based, scanning topographic / bathymetric lidar were carried out for different water bodies under different surface wave and turbidity conditions. Calibration targets were placed in the water and mapped by the lidar – see Figure E6.

Finding #14 (O2): The outdoor experiments identified known targets in shallow water (< 5 m) with centimeter-level precision illustrating in great detail natural features such as individual coral within the coral reef bed – see Figure E7.

Finding #15 (O3): The outdoor experiments experienced a range of turbidity levels in different water bodies. These levels were recorded by the same Nephelometer and an empirical curve of lidar depth to turbidity level was determined – see Figure E8. As expected through modeling, the

lidar depth performance followed a power law distribution with greater depth for decreasing NTU values.

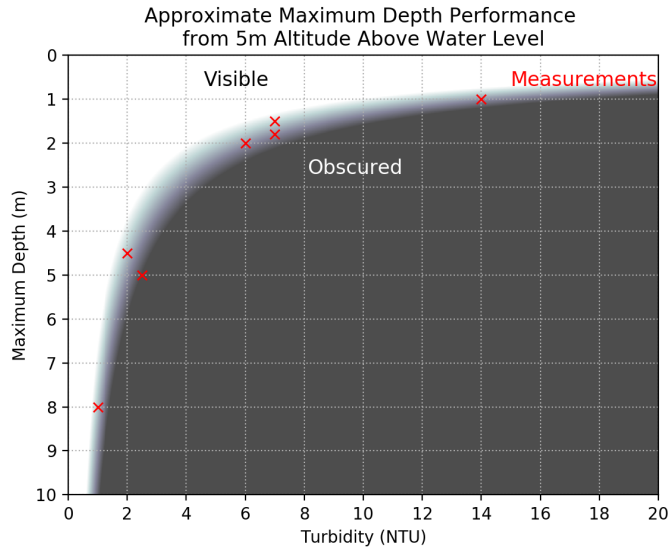


Figure E8. Lidar maximum depth performance in meters with turbidity levels in nephelometer turbidity units (NTU). The red X's indicate actual depth measurements with measured NTUs from outside experiments.

Finding #16 (O4): The outdoor experiments experienced a range of wave conditions. A sample data set off the coast of Oahu, HI consisted of breaking shore waves and wind-driven waves further from shore – see Figure E9. The lidar was able to map the sea floor in most of these wavy conditions and resolve detailed descriptions of 2 meter rocks in 4 meters of wavy surface water.

The only limiting situation occurred when foam from breaking waves scattered laser light

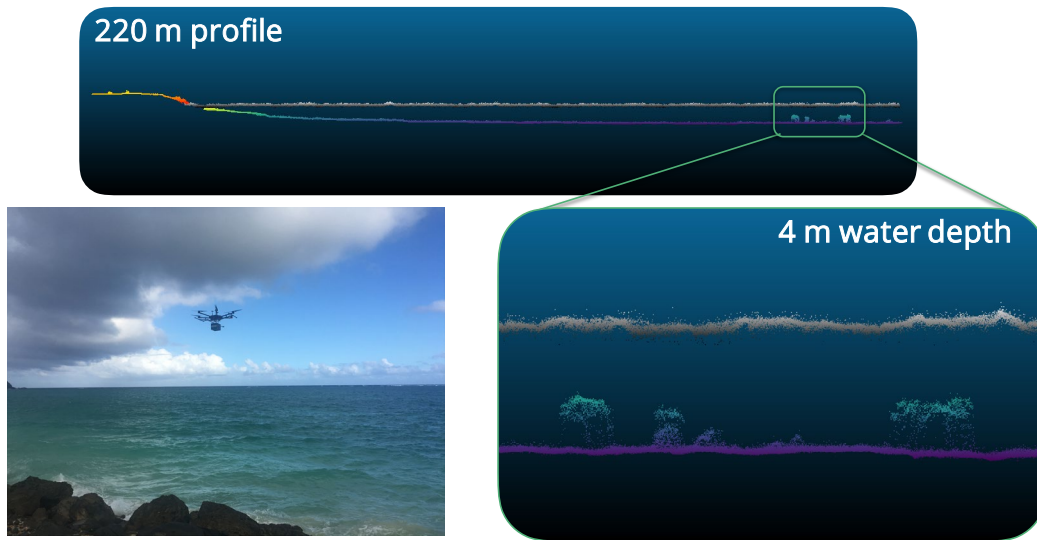


Figure E9. Outdoor experiments under wavy surface conditions off the coast of Oahu. The water surface conditions are shown in the lower left with the lidar mounted and flying on a drone above the surface. The top panel shows lidar measurements producing a 3-D mapping of land, the break wall, and the bay. The insert in the lower right provides detailed mapping of rocks submerged in about 4 meters of water depth.

preventing bottom detections and increased turbidity caused by breaking wave action.

Finding #17 (O5): The prototype, drone-based scanning topo/bathy lidar has proven the technique can work in waters expected for munitions response and, through the improved understanding of performance in wavy and turbid waters, a system could be optimally designed for such applications.

Implications for Future Research and Benefits

The findings from our modeling, lab and outdoor experiments have established that our lidar technique is practicable for detecting and identifying munitions in waters less than 5 meters deep with a total uncertainty in both vertical and horizontal resolution of < 10 centimeters. This total error is a conservative empirical precision estimate based on the culmination of error introduced by the lidar (<1 cm), platform (<5 cm), and water conditions (~1-5 cm). We understand the impacts of surface conditions and suspended material within the column on the lidar performance to properly assess its ability under different environmental scenarios. We are confident that through future research we can transition these prototype findings to an operational, drone-based, topographic and bathymetric lidar system designed specifically for munitions response.

Future Research. The SEED grant has significantly advanced the lidar technique to a level of practical use for shallow water munitions response. However, there remains several areas of research needed to make the system operational and optimal. The research involves considering further environmental conditions and system design.

Although we have addressed the effects of surface waves and turbidity on the lidar performance, other environmental issues can impact lidar operations, such as sunlight and target reflectivity. Target reflectivity has a direct effect on lidar detectability by impacting the amount of light backscattered by the object. However, we employ polarization tactics in our lidar systems which also depend on the target's polarization scattering properties. This would be an area of research to explore and better understand how targets respond in different planes of polarization.

Sunlight degrades our system performance by lowering the signal to noise in detecting under water objects. Direct and diffuse sunlight scatter have different effects on the system and methods need to be pursued to diminish sunlight scatter from reaching the lidar detectors. This would require research in the sunlight scatter expected and methods to employ in the lidar system to reduce this effect.

Another potential research area is to correct for wavy surface refraction by using the lidar to map the water's surface and fit a grid by which to correct the bottom returns based on the empirically determined wave properties.

Future research is also needed in system design for operations in such conditions as rain, humidity, heat, spray, and wind. The prototype has demonstrated capability but flight time, flight altitude, scanning coverage, measurement capability, and related design-to specifications are needed to be researched and mapped to the munitions response program's requirements. For example, research into reducing size, weight, and power would lead to longer flight times. Operating at higher altitudes would increase coverage but would require research into the design to improve performance as signal from bottom targets become weaker with greater distance from the water surface.

Integrating a camera system for data fusion between lidar and camera imagery would also be highly desirable and could enhance the measurement outcome.

Finally machine learning techniques on the retrieved lidar point cloud should be researched to automatically identify features such as water surface, water column, and underwater terrain or objects in the data and to produce real-time maps.

Benefits. The lidar-wave model and the turbidity model have proven to be very helpful in understanding observed behavior in underwater target morphometry for wavy and turbid conditions. In fact, these models will be instrumental in optimizing the lidar instrument design. Airborne lidar bathymetry parameters could be varied and tuned such that optimal performance is achieved for a given expectation of ocean conditions and environment.

The findings from this SEED grant are highly relevant to SERDP munitions response program, DoD, and science communities because this novel, above-water lidar technique could provide highly accurate ranging and mapping of submerged objects with centimeter-level precision, identify land-to-water transitions, provide accurate descriptions of bottom surface topography, object detection, object characterization, and precise water depth estimates, while eliminating risks associated with deploying traditional submerged sensors.

This lidar capability can be highly complementary to other SERDP techniques and can help provide a more complete description of the entire scene – particularly in shallow water. Like terrestrial lidar systems that determine indicators of prior munitions by detecting craters, aiming circles and other persistent surface features, the lidar technique could explore underwater bottom surface indicators of munitions activity. Providing such indicators may prove useful for quickly scanning large areas to identify likely munitions sites that will require further detailed investigation. Furthermore, mobility modeling of munitions is dependent on environmental parameters, such as water depth and bottom and top surface morphologies, which the lidar can provide as model input. The lidar measurements can also be used as a tool for designing, planning and executing surveys. An initial survey using the lidar technique can quickly provide data and insights for follow-on survey decision making, including reduction of risk to divers and other assets.

The results further address technology advancements by establishing a new technology with the ability to detect, range, and classify underwater objects with high vertical and horizontal resolution (< 10 cm) in shallow water (<5m) – without contacting the water. Relative to existing lidar systems, the resulting lidar provides unprecedented depth resolution and horizontal resolution for much improved hydrography, thus making survey results more useful. It also uses less expensive and less complex lidar components, which reduces the system cost and cost compared to other bathymetric lidar systems. The technology advancements have also led to reductions in size, weight, and power allowing for ASTRALiTe to develop the first drone-based, scanning topographic / bathymetric lidar.

Full Report

Objective

The main objective of the SEED research effort was to investigate the effects of water surface roughness and turbidity on the performance of our above-water lidar technique in detecting and classifying underwater objects in shallow waters (< 5 meters). The technical objectives of the SEED grant are specified by the following tasks/criteria in the order they were carried out. These deviate slightly from the original task list to better organize activities and results.

Task 1) Incorporate Water Surface Roughness into Lidar Models: This task required advancing lidar simulations to evaluate theoretically how surface waves will effect lidar performance.

Task 2) Incorporate Water Turbidity into Lidar Models: This task required advancing lidar simulations to evaluate theoretically how water turbidity will effect lidar performance.

Task 3) Measure Effect of Turbidity: This task required a controlled lidar experiment of depth measurements while introducing known properties of suspended particulates to evaluate optical propagation through particles of known size and concentration.

Task 4) Measure Effect of Waviness of Water Surface: This task required the construction of a small wave tank and lidar detection system to perform controlled indoor experiments that illuminate the effects of wave amplitude and frequency on the lidar's accuracy and precision in describing underwater objects.

Task 5) Outdoor Environmental Test: This task required the deployment of a prototype lidar system over water bodies of various conditions to demonstrate outdoor capabilities.

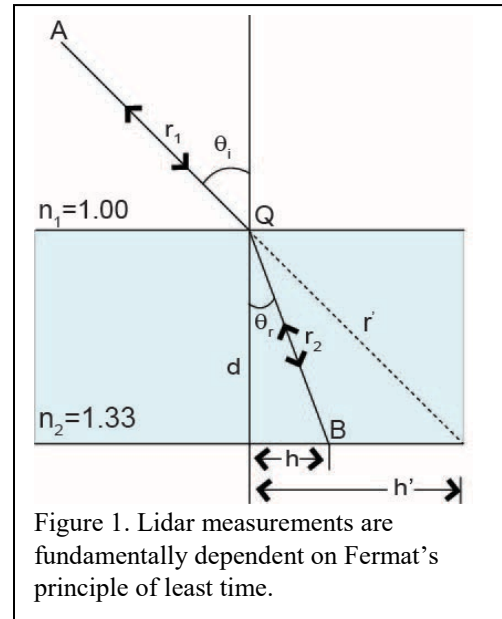
Background

As described in the Statement of Need (SON) in the Munitions Response (MR) program area, MRSEED-18-S1: Detection, Classification, and Remediation of Military Munitions Underwater, the problem to be addressed is to develop technologies to detect, classify, and remediate military munitions found in aquatic environments. A specific need is for technology to operate in depths less than 5 meters: where munitions of interest may be found in a wide variety of aquatic environments, such as ponds, lakes, rivers, estuaries, and coastal areas; where munitions are likely to be encountered by the public; and where mobility of munitions is expected to be an issue. Target morphometry (the ability to accurately determine the dimensions - length, width, and height of targets identified compared to the known dimensions of these same targets) and target positioning (the ability to accurately determine the specific location of targets) are primary methods for reacquisition and remediation of underwater unexploded ordnances (UXOs). Sensors considered previously for addressing this need include electromagnetic induction (EMI), magnetic, optical, sonar/acoustic, chemical sensors, and laser line scanning sensors (LLSS). Platforms include autonomous underwater vehicles (AUVs), remotely operated vehicles (ROVs), and towed arrays. Navigation and positioning technologies include long base line (LBL), ultrashort baseline (USBL), Doppler velocity log (DVL), real-time kinematic global positioning system (RTK-GPS), and inertial navigation technologies.

Many acoustic systems, such as high-frequency towed or hull-mounted side scan or multi-beam sonar systems, do not perform optimally in water depths shallower than 5 m where issues associated with multipath, narrow beam widths, navigation and positioning with waves, and currents limit performance. In these shallow depths magnetic and EMI systems that crawl, or are towed across the bottom, are employed but their effectiveness is limited in resolution, noise contamination, and operations. Optical systems producing 2-D imagery have been demonstrated, as have LLSS. **However, these systems, along with the others, require submergence in water, and these shallow regimes create unique challenges in access, navigation, deployment, viewing, and sensor standoff distance. Furthermore, changing bottom topography or obstructions pose a risk to equipment and personnel due to the dynamic shallow-water environment.** Thus, new technologies need to be explored to adequately address this challenging problem and likely the solution will need to operate out of the water.

Above-water lidar bathymetry has demonstrated its utility for measuring water depth and mapping subsurface terrain [Guenther et al., 2000a; Guenther and Maune, 2007] in deep waters. Lidar bathymetry systems operate onboard platforms such as helicopters and fixed-wing aircraft, collecting bathymetric measurements for use in coastal water research, nautical charting, and reconnaissance efforts [Pe'eri and Long, 2011; Brock and Purkis, 2009; Churnside et al., 2001; Guenther et al., 2000b; Irish and Lillycrop, 1999]. For bathymetry applications, the time lapse between the detected surface and bottom returns provides an estimate of the optical path length through the water, or the target range, after accounting for the different light propagation speeds through air and water (i.e., differences in the index of refraction). The water depth of the target and its horizontal position can be estimated from the water path length measurement and correcting for refraction given information on the incident angle of penetration. A major limitation to conventional lidar bathymetric measurements is their inability to operate effectively in the shallow-water domain [Guenther and Maune, 2007; Allouis et al., 2010; Pe'eri et al., 2011]. This limitation is caused by challenges in adequately separating the water surface from the bottom surface and detector blindness through strong surface returns. Detector blindness causes the detector to be nonresponsive for a duration longer than the time it takes for the laser light to two-way travel through the water path length between surface and underwater object. This detector blindness and lack of range resolution results in most systems operating in deeper waters where the resolution is less stringent and there is sufficient time for detectors to recover from the surface return. Our novel lidar technique mitigates these effects offering a solution for shallow-water observations of underwater objects. Although a major advancement, there remain challenges in understanding how water conditions may affect the performance of the lidar technique and, thus, is the topic of this research project.

The ability to perform high-resolution ranging from above-water lidar measurements of features and objects in shallow waters requires the ability to detect scattered signals from the surface and submerged objects quickly, and to precisely estimate their time-of-flight (ToF). Lidar operates in the time domain based fundamentally on Fermat's principle of least time – light travels the path in which it can reach its destination in least time – see Figure 1. This principle is used to derive Snell's law from which the range can be estimated. Based on this principle, an above-water lidar's ability to accurately determine the position and dimensions - length, width, and height - of a submerged target, or map underwater bathymetry, depends on signal detectability, pointing knowledge, and timing precision. A 3-D image of the underwater object can then be formed by rapid scanning, high laser pulse repetition rates, and platform motion, i.e. aircraft or drone.



In contrast to 3-D images produced by above-water lidar using time correlation, passive optical imaging techniques for 3-D reconstructions, such as structure from motion (SfM) and stereo imaging, from above the water surface rely on spatial correlation between points and suffer from distortions produced by wavy surfaces, turbidity, and illumination. These techniques often rely on static and unobstructed views of targets with many contrasting features (edges, colors, shapes, etc...) so they can be used as fiducial points by which to track through the image reconstruction process [James and Robson, 2012]. Water is neither static nor unobstructed making 3-D imaging of underwater objects obscured and distorted. Water surfaces act like a constantly-changing lens for optical imaging systems. These distortions correspond to affine transformations between the true scene and what the sensor captures. The challenge with distortions caused by the medium is that the objects behind or inside that medium are shifted due to refraction causing translation, rotation, and scaling effects. Surface waves can create shimmering lines that show up in imagery and can both obstruct real features used for tracking and register as features themselves in SfM techniques. When the illumination source(s) of the scene is not controlled, the image is susceptible to such affects as glint (obscuring objects under the glinted region or registering as a feature in the scene) and illumination variations (caused by clouds, shade, water turbidity) that impacts signal-to-noise and the overall performance of detecting a target. Finally these approaches can only be applied during the day.

Lidar is less affected by many of the issues that plague above-water optical 3-D imaging of underwater objects, but water conditions do impact the lidar accuracy and precision of object morphology. Detectability, pointing knowledge, and timing are lidar system attributes required for 3-D imaging whose precision is impacted by the conditions of the water. Two water conditions important to above-water lidar performance are surface waves and turbidity. Surface waves affect 1) water-surface detectability by surface reflections steering signal out of the lidar

receiver's field of view, 2) pointing knowledge with respect to the water surface by inducing variability in the laser light incident angle on the water's surface, and 3) timing uncertainty by changing the water depth in an unknown amount causing uncertainty in water path length. Our wave-lidar modeling and experimental procedures illuminate these effects and provide quantitative assessments of their impact on describing and characterizing submerged objects.

Turbidity in the water column affects detectability of submerged objects by extinguishing laser light as it propagates through the water column. There is a large body of work that describe and pursue the measurement of turbidity in water columns. An excellent compilation of measurement techniques and theoretical descriptions of turbidity in water is given by Jonasz and Fournier [2007]. Turbidity in ocean waters can cause signal attenuation over many orders of magnitude [Mobley, 1994]. In lidar, this must be considered for both the outgoing and returning paths. The reduction in laser light can be caused by absorption and scattering by particulates suspended within the water column. Absorption removes photons permanently from the laser light while scattering causes the photons of light to be redirected and potentially out of the lidar's viewing angle. Absorption by water molecules can be addressed straightforwardly, although there is some dependency on temperature and salinity, but particulate absorption is highly dependent on the composition, concentration, and spectral properties of the particulate matter. Scattering is less spectrally dependent but can produce complex angular scattering effects that depend particularly on shape, concentration, and particulate size relative to the laser wavelength [Bohren and Huffman, 1983].

In addressing the effects of turbidity on lidar signals for this SEED activity, our approach focused only on the influence of scattering by particulates of different size and concentration suspended within the water column, not on particulate absorption. This does not presume that absorption is not an important factor in total laser light extinction but we chose to focus on scattering to isolate its effect on lidar signals and make the modeling and experimental results more tractable. Our Monte Carlo modeling effort employs Mie theory [Bohren and Huffman, 1983] to describe the scattering process whereby dielectric spheres with complex refractive indices and variable size parameters are distributed within the water column. A Monte Carlo program has an advantage over many other types of radiative transfer simulations because it requires very few simplifying assumptions or approximations. This allows for calculations involving complex media (varying densities or particle identities) and complex geometries. Another advantage is that the problem can be broken up and analyzed at each step so contributions from single, double, and higher-order scattering orders can be separated. Added flexibility comes at the price of computation time and resources, although as computers increase in speed it is becoming more feasible to perform complex calculations

The effect of water conditions involving wavy surfaces and turbidity on lidar performance are the focus of this SEED project.

Materials and Methods

The technical approach used a variety of materials and methods involving simulation, controlled lab experimentation, instrument prototyping, and outdoor experiments to meet the research objectives. Simulations included a Monte Carlo scheme that followed photons as they

propagated through turbid media and a ray trace scheme to map the effects of surface reflection, transmission, and refraction due to wavy surfaces. Indoor experiments were carried out using the lidar technique with a graduated cylinder and a water tank to determine turbidity and surface wave effects on lidar measurements. A prototype lidar system was also used to demonstrate outdoor capabilities.

Task 1) Surface wave simulations: The surface-wave-lidar model incorporates a realistic ocean surface model with a lidar ray-trace scheme that simulates the lidar beam interaction with a wavy surface. A large number of beamlets makeup the lidar beam. Each beamlet is ray-traced and refracted through the water using an instantaneous value for the wave slope at the beamlet intersection of the water surface. The beamlet entrance point and bottom point are registered to illustrate the effects of the wavy surface on the beam propagation. A treatment of georeference frames has also been included to simulate a lidar mounted and moving on aircraft that include GPS and an inertial measurement unit (IMU). Another aspect of light propagation included in the code is treating the polarization of the laser light and performing the necessary polarization transformations to properly address the alterations of polarization upon reflection and transmission through the wavy surface.

With the combination of an ocean surface model and an airborne lidar bathymetry (ALB) model, a variety of simulations can be done in order to better understand the effect of waves on ALB measurements. Simulations have been conducted to show the capabilities of the model and to observe how the ocean surface can affect ALB measurements. A typical simulation included the

use of the Joint North Sea Wave Observation Project (JONSWAP) spectrum [Hasselmann et al., 1973] with the following set of parameters: the wind speed was set to 6.0 m/s, the grid resolution was 256 in x and y, the grid size was 75 by 75 meters, the dispersion relation was set to shallow (the ocean depth was 2m). For the lidar, the beam divergence was 0.1 degrees, the average pulse power was 20 mW integrated over 14 kHz laser shots, the wavelength was 532 nm, the FWHM of the laser beam leaving the lidar was 0.5 mm, the ray distribution was radial, and the beam power distribution was Gaussian. These parameters are similar to those exhibited by one of our lidar systems. Figure 2 is an illustration of the various attributes of the model and the effect of the wavy surfaces on beamlets projected on the ocean bottom.

As for reference frame settings, the lidar was mounted and directed along the yaw axis of the aircraft and the aircraft was aligned with the North, East, Down frame. The lidar was offset by 10 degrees in pointing angle of the simulated surface grid at 500 meters height above the surface. Other configurations are possible and aircraft motion can be included in the simulation. For this simulation, the aircraft and lidar are effectively suspended above the water surface. The results of this simulation are shown in the lower panel of Figure 2. The total beam was simulated with 60 beamlet rays but only a select few are displayed. The red dots represent the beamlet position at the original flat-surface grid. The blue dots indicate the position on the bottom surface after the rays experience water surface refraction and propagation through 2 meters of water. The bottom surface is presumed flat.

To extract depth and horizontal position of objects on the ocean floor, the incident angle at the surface and water path length must be known. This is illustrated in the Figure 2

2-D JONSWAP wave spectrum

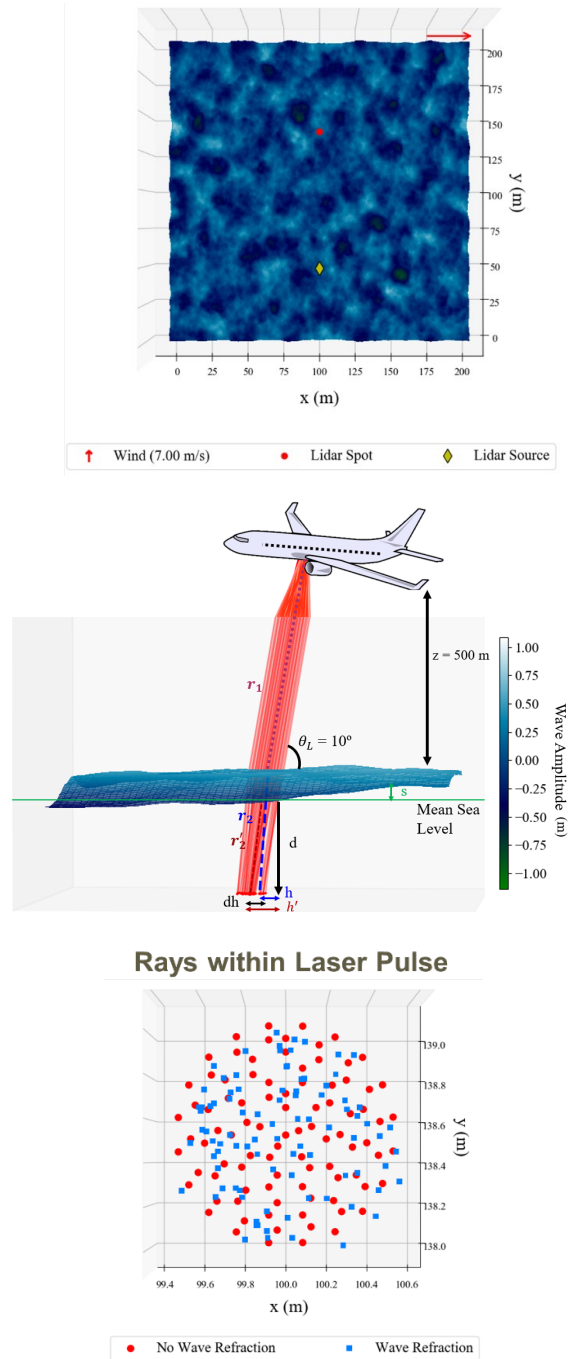


Figure 2. Combined surface wave spectrum (2D JONSWAP) and lidar simulation for individual beamlets within the laser beam. The wind speed is 6 m/s and the water depth is 2 meters. The lidar is airborne at 500 meters pointing nadir and the bottom panel shows the projection of beams on the ocean bottom.

diagram of ALB measurements where the range to the surface is r_1 . The range from the surface to the floor without knowledge of the wave slope (this assumes the surface is flat) is r_2 . The true range from the surface to the floor is r'_2 from which depth can be derived. The difference between the horizontal position of the surface detection and floor detection is h . Given an off-nadir angle, this can be estimated by once again assuming the surface is flat. In reality, refraction changes this to h' . The horizontal position error is therefore dh . In the presence of waves, both the incident angle and water path length vary causing estimates of depth and horizontal position to also vary. This variability translates to timing uncertainty in the lidar measurement.

Figure 3 plots a timing histogram for each beamlet that is propagated in the laser beam path for the simulation described above. The true depth is shown in red but the signal is spread asymmetrically where a bias towards estimating deeper water is introduced due to variations in wave slope and wave height. The distribution spans about 5 cm and the bias is about 2 cm. This outcome is very dependent on the wave conditions and lidar system parameters.

It should be noted that the model results presented above are specific to lidar system parameters. Variations in lidar parameters (such as, laser divergence, pointing angle, lidar elevation) are easily adjustable within the model and may have notable effects on how the waves affect target morphology. For example, a lidar with a spot size greater than the wavelength of the water waves will not experience refraction solely in one direction. Additionally, surface height variations within the beam footprint will have a sizable effect on timing and therefore range uncertainty. For this situation, the added uncertainty in the cross-range and range directions may be different.

This forms the concept that the lidar-wave model could be used for instrument design. ALB parameters could be varied and tuned such that optimal performance is achieved for some given ocean conditions and environment.

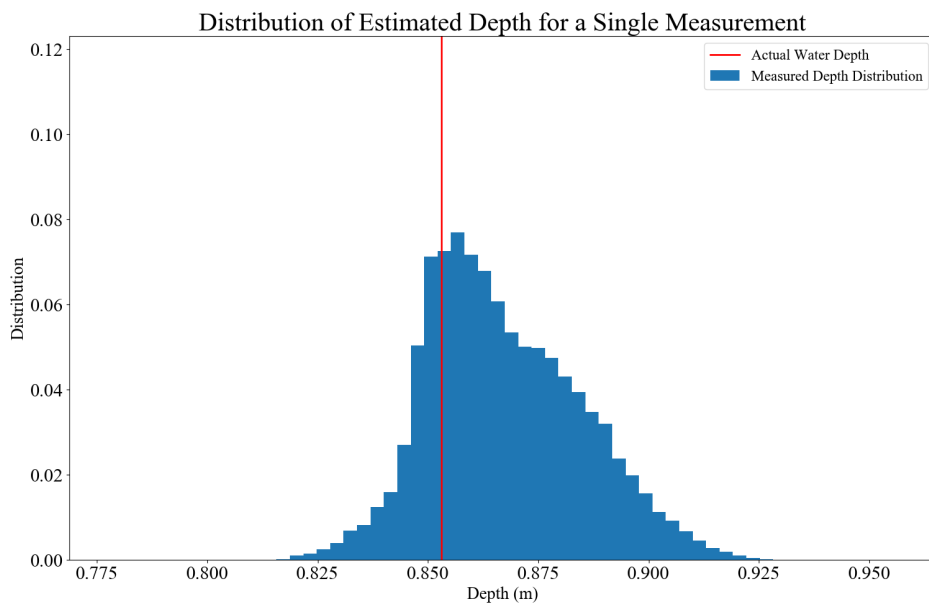


Figure 3. Simulated lidar beamlets time of flight distribution from a flat bottom surface refracted through a wavy surface.

Task 2) Turbidity simulations: A 3-

D Monte Carlo model, the ASTRALiTe Monte Carlo Lidar Simulation Tool (MCLST), has been developed to simulate laser light propagation through turbid water. This model takes a different approach than the ray-trace wave model presented above. Here, single photons are propagated through multiple scattering events in the water column while retaining polarization information at each stage. The model tracks laser polarization using Stokes vectors and Mueller matrices to calculate polarization effects due to scattering. Various lidar (beam size, divergence, polarization state, wavelength) and environmental (particulate size, particle density, index of refraction, absorption)

variables can be adjusted in the model to fully explore the trade space of lidar parameters and environmental conditions. In the simulations photons from the lidar laser pulse are propagated through the water medium with uniformly distributed particulates of different particle size relative to the laser wavelength. For these simulations the water surface is not considered so any effects on the beam is solely due to the water column and the presence of a specified type of particulate in the water. The simulation is based on optical depth not physical depth to allow for the outcomes to be adequately compared with other simulations of different particulate types. Figure 4 shows the outcome of propagating laser light through turbid media. The beam is scattered horizontally as it propagates into the water causing beam spread and a reduction in beam intensity with distance as the photons are scattered out of the lidar receive path.

Task 3) Turbidity experiments: Experiments to validate the turbidity propagation model were performed by mounting a stationary lidar system over a graduated cylinder to identify the effects by carefully controlling turbidity levels in a controlled environment. To match the model's conditions as closely as possible, a calibrated quantity of particles of uniform size and material are incrementally introduced into pure water and thoroughly mixed – see Table 1. We used two types of calibrated particles: a) Cospheric brand monodisperse silicon dioxide microspheres with index of refraction 1.47, size distributions $CV < 6\%$ for sizes 507 nm, 1.18 μm , and 9.2 μm and b) Bangs Laboratories, Inc brand polymer microspheres with index of refraction 1.57, with ± 10 nm size distribution for 25 nm and 100 nm. Our test bed is a 500 mL graduated cylinder creating a water column that is 24.1 cm tall to give medium water depth while conserving the turbidity-creating particles – see Figure 5.

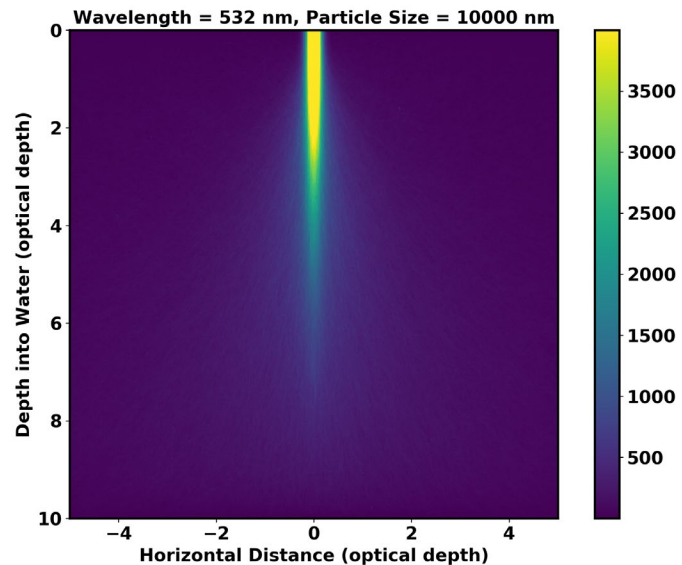


Figure 4. MCLST simulation of optical depth penetration and spreading of a lidar beam propagating through the water column with a uniform distribution of 10 micron spherical particles.

Table 1. Calibrated Particles

Particle Size (µm)	Particle Material	Index of Refraction
0.025	Polystyrene	1.57
0.100	Polystyrene	1.57
0.507	Silica	1.47
1.18	Silica	1.47
9.2	Silica	1.47

A full set of turbidity experiments were completed using an existing, polarization sensitive, stationary lidar system. The experimental setup places the lidar transmitter/receiver above the water body and directed near nadir to the water surface. The receiver is aligned along the same optical axis to receive the laser light after it has propagated into the water column and reflected back from the bottom surface. The lidar receiver records signals from the air-water interface and the water-bottom interface in two planes of polarization. Data from both polarization channels have been processed however, by design, only the perpendicular channel, or cross-polarization channel, is used in the analysis. A constant bottom reflectance is maintained throughout all experiments in order to observe only changes in the water column due to the introduction of suspended particles. The lidar signals recorded during these tests have been processed to extract information regarding the effects of turbidity. Namely, the amplitude, peak return time, and width of the peaks in the received lidar signal from the water surface and the bottom.

The microspheres allow for consistent optical scatter that is evenly distributed throughout the water column from materials with known optical properties such as sphericity, index of refraction, and absorption. These are all properties that are inputs to the MCLST turbidity model. Carefully measured quantities of the microsphere particles are manually mixed into 500 mL of Type I water contained in a clean graduated cylinder. For verification, the water turbidity has been measured with our Nephelometer and recorded in Nephelometer Turbidity Units (NTUs). The turbidity of each concentration is measured in NTUs to build calibration curves to a standard measurement for future comparison to the more complex natural environment.

Task 4) Surface wave experiments: Indoor surface wave experiments were carried out using an in-house wave tank built and tested by ASTRALiTe engineers. The tank is able to generate a range of different water waves consistently over long periods of time with minimal effects due to

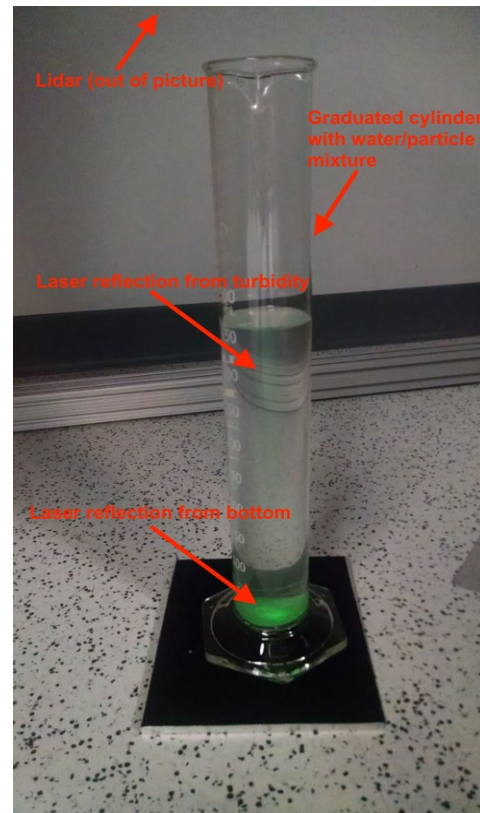


Figure 5. Image of the lidar-turbidity test setup. The lidar beam can be seen interacting with the turbid water sample. Not pictured is a black cover placed around the inside of the cylinder to prevent reflections.

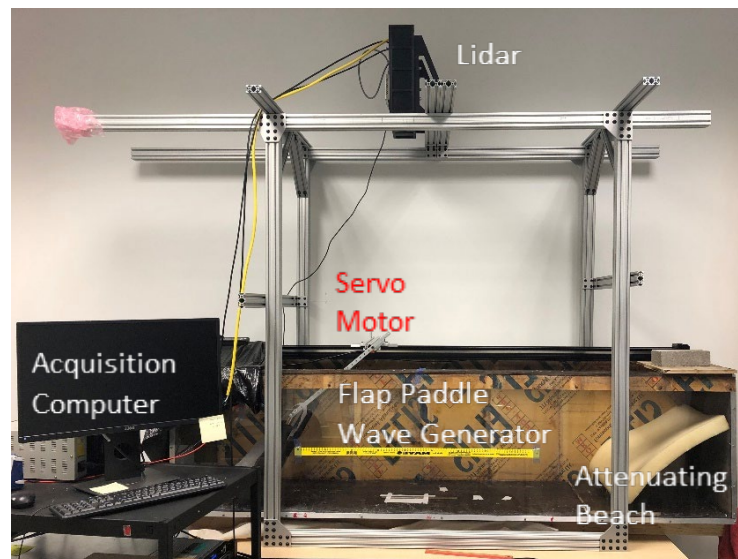
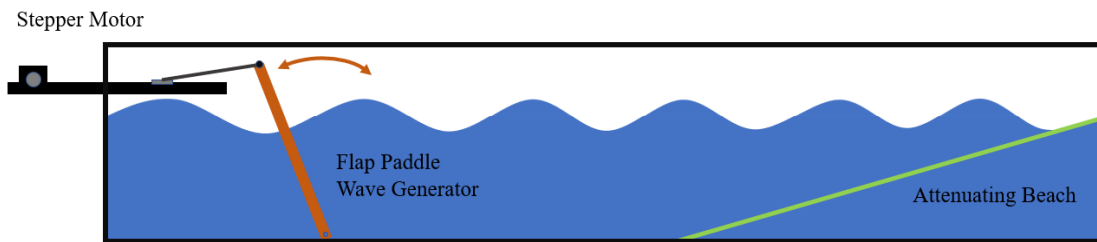


Figure 6. Design of a small wave tank using a flap paddle driven by a rail mounted stepper motor to generate waves of specific wavelength and amplitude. An absorbing beach is placed at the back of the test tank to prevent wave reflections. A sample of actually waves generated in the tank with a measured wavelength of ~ 29 cm. The target wavelength for this test was 29.5 cm.

reflections at each end or by the walls. The tank has been shown to be capable of generating waves between 0.12 and 0.7 meters in wavelength – see Figure 6 for setup and example. Additionally, at each wavelength the shape and amplitude of the waves can be controlled. The wave-generating motor used in the final design is a powerful servo that can create waves at high frequencies. In addition to the tests listed above, there is the capability to superpose sinusoids representative of a realistic ocean spectrum. The results from these tests will be compared to the lidar-water-wave model described in task 1. This will serve as validation for the model, which can then be used to predict and understand lidar behavior in the instance of more complicated water surface structure.

Task 5) Outdoor experiments: ASTRALiTe's engineering team designed, built, tested, and flew a prototype scanning topographic / bathymetric LIDAR system aboard a DJI Matrice 600 Pro drone through a separate funded project. The payload weighed 5 kg and included the lidar, IMU, GNSS, camera, and hour-long batteries. ASTRALiTe constructed the entire instrument package including an entirely new acquisition system to enable high-resolution (20 picosecond) timing, resulting in a range resolution on the order of 1 cm. The lidar system is coupled with an IMU with dual GPS antennas that facilitate high accuracy real-time and post-processed position and attitude measurements. The scanning approach employed on this system is a push-broom approach so that as the UAV flies at altitude an area is mapped out. The swath width of the lidar map is about half the flight altitude. A series of outdoor experiments were conducted and offered the opportunity to test performance under actual conditions of wavy and turbid waters.

Results and Discussion

This section combines the simulations and lab experiments to explain and present findings on the effects of surface waves and turbidity on lidar performance. Outdoor experiments are also presented that demonstrate the potential capability of this technology to detect underwater munitions in shallow waters (< 5 m). These measurements experienced both wavy and turbid conditions and provide empirical evidence for the technique's ability to operate in environments relevant to munitions response.

Surface wave effects

The lidar-ocean surface model developed for this program, and presented in the previous section, can represent very complex and realistic surface structures. Additionally, this model can handle a range of different lidar parameters and ALB scenarios. This model has already shown that different water surface conditions can have a significant effect on lidar bathymetry by spreading, focusing/defocusing, delaying, and refracting the lidar beam. The experimental wave tank setup can generate a range of wavelengths and amplitudes and has the capability to superpose sinusoids to represent a realistic but scaled ocean spectrum. However, to compare the wave tank tests with the model, the wave structure generated by the model was changed from one based off the JONSWAP spectrum to a single sinusoid. This closely represents most of the waves generated in the wave tank experiments.

Target Morphology of a Submerged Brick:

To investigate how an underwater target is distorted and changed when measured by the lab lidar through a wavy water surface, a brick was placed on the tank floor in about 26 cm of water and the lidar was moved incrementally by 1 cm down the tank as waves were generated. The waves generated for this test were 35 cm in length and approximately 1.5 cm in amplitude (3 cm peak to peak). The experimental setup was the same as that presented in Figure 6. An image of the lidar range points detected through the wavy water surface with the brick dimensions superposed is given in Figure 7. This image shows some of the main affects water waves impose when it comes to target morphology. The edge of the brick, which would normally be sharp and well defined is now blurred. Return signal from the tank floor and from the brick top overlap near the brick edges. Additionally, there are detections coming after the actual range to the brick surface and tank floor. The plot indicates that the cross-range uncertainty caused by waves is more significant in this experiment than the changes in the range distribution with several centimeters of uncertainty adding horizontally by the waves. Model results confirm the edge of the brick to experience blurring and the range to the brick and floor are varied with a slight bias towards a deeper depth. The model shows that the deeper bias is introduced as a nadir viewing lidar will always experience greater path lengths due to refraction caused by the sloping waves. The

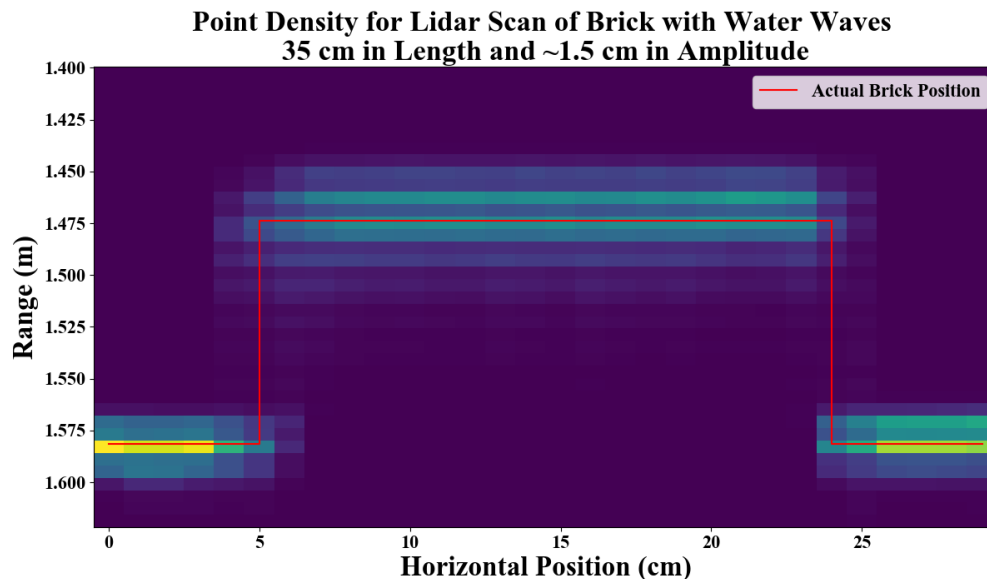


Figure 7. Lidar scan of submerged brick in 26 centimeters of water. The number of detections with range is displayed using a normalized color mapping. The actual brick shape is also shown for reference in red.

variability in the range is attributed to changing wave amplitudes that result in the different timing delays as the light travels through more or less water depending on whether a crest or trough is present, respectively.

Full Set of Lidar-Wave Tests:

Given the potential for different lidar responses under different wave conditions, a more statistical approach was taken where a wide range of wavelengths and amplitudes were produced in the wave tank while the lidar ranged to the bottom of the tank. The amplitude of these waves was selected to match the significant wave height of the wave tank waves to the significant wave height calculated using the JONSWAP spectrum. Tests were done at the following wavelengths: 12 cm, 18 cm, 25 cm, 30 cm, 35 cm, 40 cm, 50 cm, 60 cm, 70 cm. At each wavelength, at least two different amplitudes were tested. For some of the medium sized wavelengths, three amplitudes were tested as the medium sized waves were the ones most easily produced by the wave tank. Overall, 22 tests were performed and a scaling factor of 70 was determined to best map wave tank waves to ocean waves whose wavelengths would span from 8.4 to 49.0 meters in length.

For wavelength and amplitude, two tests were done with the lidar recording data off the tank floor, and one test was done with the lidar measuring the water surface. The water surface data was obtained by placing a thin film over the water in the region local to the lidar beam. The lidar

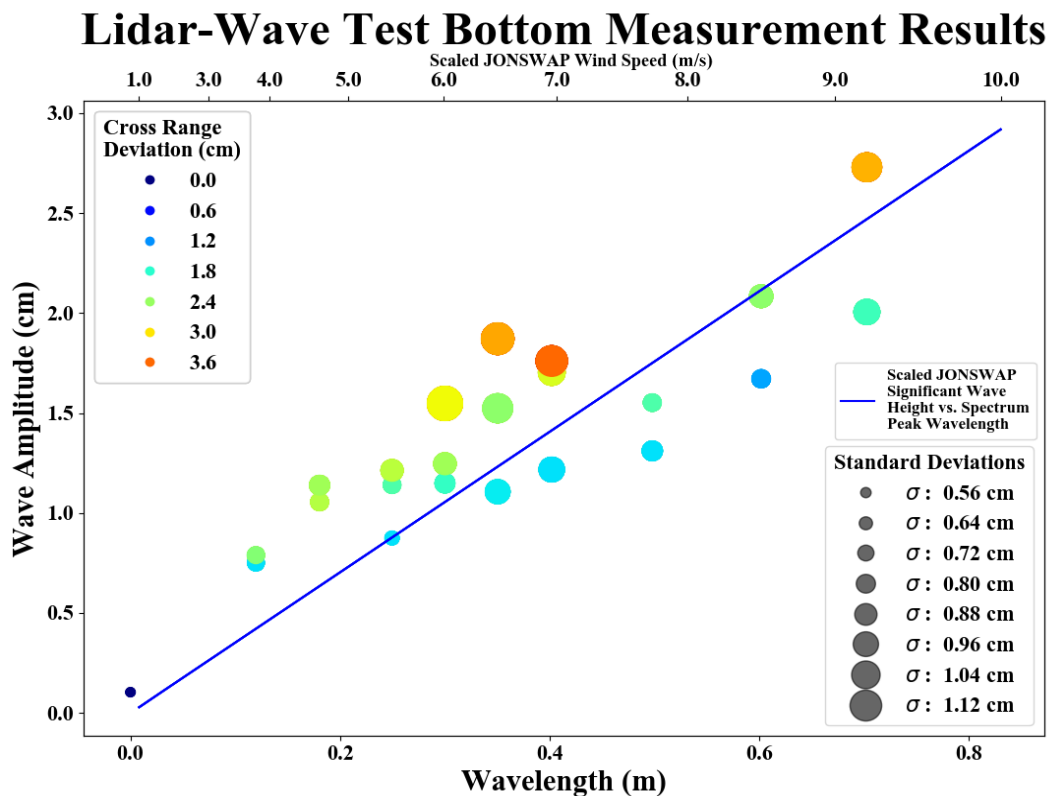


Figure 8. Graph showing many of the results for 22 different wave tests of different wavelength and amplitude. Each scatter plot point is its own wavelength and amplitude. The size of each point refers to its increase in standard deviation from its nominal, still water distribution. The color of each point represents the horizontal deviation caused by the waves. The JONSWAP significant wave height and peak spectral wavelength are also plotted with the scaling factor of 70 applied. The wind speed that corresponds to each JONSWAP peak wavelength is also shown at the top of the plot.

surface data was used to determine the actual RMS amplitude of the waves. The tank floor range data was processed in order to find the standard deviation. Additionally, the maximum cross-range deviation in both the direction of wave travel and against it was recorded. This was done visually using a ruler mounted on the inside of the tank next to the lidar beam spot. The results of these tests are shown below in figure 8.

Several interesting features can be observed on this plot. First and foremost, the amplitudes of the generated waves closely adhere to what would be expected from the JONSWAP spectrum after applying the scaling factor. This means that the waves generated during this experiment were close to what would be seen if the JONSWAP spectrum was collapsed to a single wave with winds ranging from 3-10 m/s. A real ocean surface has energy superimposed at a wide range of wavelengths and as such is much more complicated than the surfaces produced for this experiment. Nonetheless, the waves tested and analyzed in this section should be about as representative of typical ocean behavior as a single sinusoidal wave can be.

The relationship between cross-range deviation and the wave amplitude/length is another important feature displayed on this plot. This relationship shows how the lidar's ability to resolve bathymetric targets is affected by waves of different lengths and sizes. The general trend displayed in figure 8 is that the cross-range deviation is related to the wave amplitude for specific wavelengths. In other words, a larger amplitude relative to the wavelength of the waves results in more cross-range deviation. This is a sensible result seeing as this basically can be equated to steeper waves which will cause more off-nadir deviation due to refraction. We can also see some influence due to waves losing their perfect sinusoidal shape. This is especially evident for the high amplitude waves with length between 0.3 and 0.4 m. These were some of the steepest waves generated in the tank and they began to take on a sort of "peaked" shape. For these waves, the slope near the wave peak was much larger than what would be expected for purely sinusoidal waves of the same length and amplitude.

The range uncertainty also determines how well underwater targets can be resolved by the lidar. The lidar range uncertainty is generally closely tied to the standard deviation of the lidar detections in range. This is shown in figure 8 using the diameter of the points in the scatter plot to indicate the relative size of the standard deviation, as indexed in the lower right corner. The relationship between the range distribution and the wave parameters is slightly more complicated than with the cross-range deviation. While the cross-range deviation was affected solely by the wave slope and refraction, the range standard deviation is affected by both refraction (increasing path length) and by the fact that the lidar beam will be travelling through more or less water depending on whether a wave peak or valley is passing through the beam spot. As can be seen from figure 7, most of the low standard deviation tests are concentrated below 0.3 m in amplitude. This indicates that likely the dominating factor influencing the range standard deviation is not refraction but instead the added transit time through water due to the wave geometry. This idea is supported by the fact that for a single wavelength, the dots seem to increase in size as amplitude increases. As with the cross-range deviation data, the high amplitude tests with wavelengths between 0.3 and 0.4 m have the largest range uncertainty. This

is not surprising seeing as these tests have the largest cross-range deviations and also some of the largest amplitudes.

In terms of target morphology with a nadir-viewing lidar, this plot indicates that the cross-range error is the more significant source of error in the presence of a wavy water surface. Figure 7 also supports this claim. The brick is not well resolved in the horizontal direction in Figure 7 however the top of the brick and the tank floor are still quite clear. However, this influence will vary as the lidar beam is steered off nadir.

Comparison to Model:

The lidar-wave model was run for each of the wavelengths and wave amplitudes tested in the preceding section. Using the wave model, the lidar range distribution and beam centroid

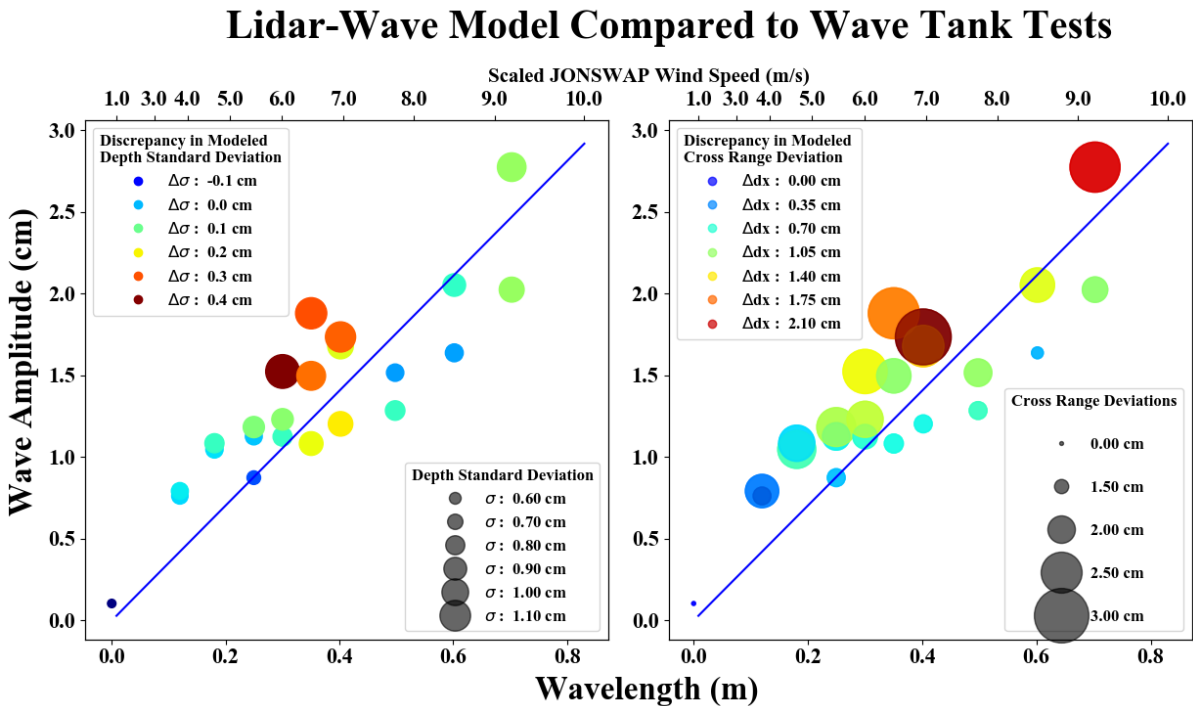


Figure 9. Scatter plot of all wave tests colored by the discrepancy between the actual test and the lidar model. On the left is the discrepancy in range standard deviation. On the right is the cross-range deviation. The points are sized according to either their respective standard deviations or cross-range deviations. As with figure 7, a line denoting the corresponding scaled JONSWAP significant wave height and peak wavelength is plotted versus wind speed.

deviation were simulated. By comparing these results to the experimental test results, we can see how well the model represents the data statistically and where limitations may exist. In order to understand how the model compares with the tank tests, a plot similar to figure 8 was generated in Figure 9 with the left plot comparing range deviations and the right plot comparing cross range deviations. Overall, the lidar-wave model does a better job of representing the range standard deviation as opposed to the cross-range errors. The range errors estimated by the model deviate from the observations by only a few tenths of a centimeter with the depth standard

deviation being similar to what was observed in Figure 8. The cross-range differences are on the order of a centimeter with the model experiencing more deviation than observed. The cross-range errors are primarily driven by the wave slope whereas the range standard deviation was driven mainly by the variations in transit time due to the laser light having to travel through more water due to the wave. This implies that the model is doing a good job of replicating the water surface shape however it is missing some slope variation. This slope discrepancy can likely be attributed to small, capillary wave structures. These small waves could be seen in the tank during testing and were likely caused by tank imperfections and edge effects. Some of the missing slope variance is also likely due to the waves losing their perfectly sinusoidal structure. This is especially evident for the high amplitude tests where the peaks of the waves became quite sharp. In some cases, the waves were even nearing the point of breaking in which case the wave slope will become unpredictable and much larger than expected. From the cross-range discrepancy side of figure 8 we can see that the model does a good job of capturing the cross-range deviations for small amplitude waves. The model discrepancy is greatest for the waves with large wavelengths and large amplitudes. These waves were often times the ones with the most significant capillary and non-sinusoidal behavior.

For the range standard deviation, it can be seen that the model does a good job everywhere except for the high amplitude tests in the 0.3 – 0.4 m wavelength region. This is likely due to the aforementioned conjecture that these waves are not very sinusoidal. An additional source of error that has not been mentioned and is related to the waves not being perfect sinusoids is that the root-mean-square to amplitude conversion used in this analysis is only true for perfectly sinusoidal signals. For more triangular waves, such as those corresponding to the 0.3-0.4 m wavelengths, the formula would underestimate the wave amplitude. This means it is possible that the high amplitude wave tests between 0.3 – 0.4 m exaggerate the effect of increased range standard deviation due to the changing path length corresponding to the wave peak and troughs.

For further validation, a direct comparison is made between the lidar data ranging histogram (a fundamental measurement by the lidar where every recorded beamlet time-of-flight is converted to range) and the simulated ranging histogram using the model for a specific wavelength and amplitude. The results of this comparison are shown below in figure 10. The model performs well and demonstrates many of the data features observed.

Lidar Range Distribution for 30 cm Waves with ~1 cm Amplitude

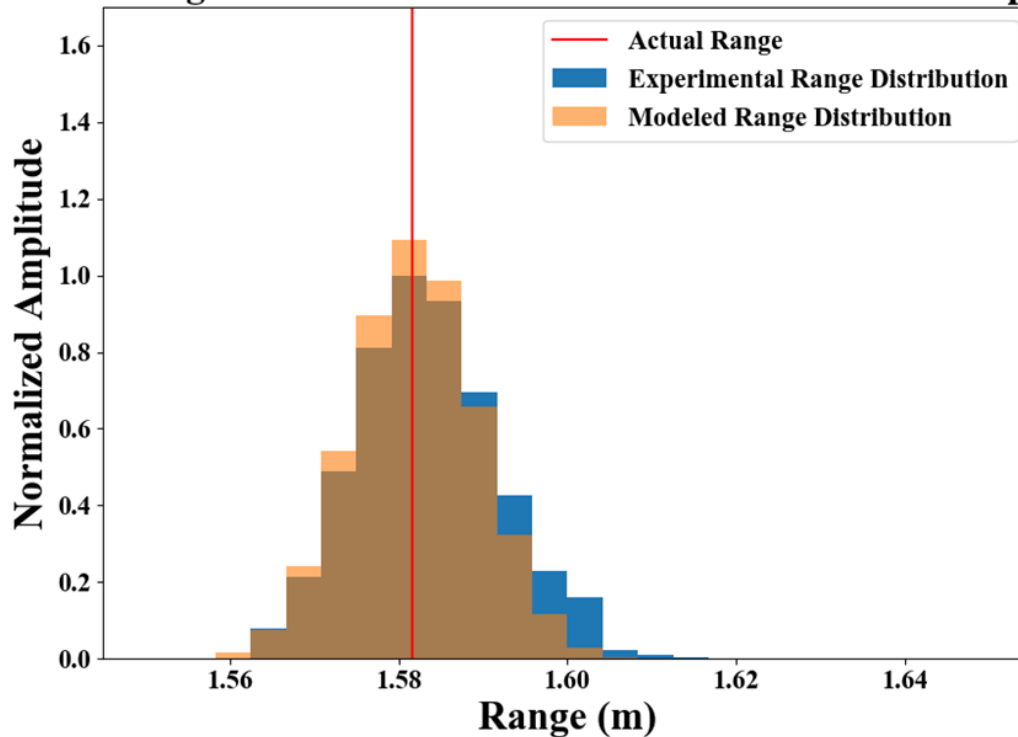


Figure 10. Comparison between modeled lidar range distribution and experimentally measured lidar range distribution for lidar aimed at tank bottom with 30 cm waves at ~1 cm amplitude.

The following is a summary of findings for surface wave effects (W#) on lidar performance.

Finding #1 (W1): A surface wave-lidar model has been developed to assess the influence of waves on the lidar's ability to determine the dimensions of an underwater object. The model incorporates a realistic ocean surface wave model with a lidar ray-trace scheme that simulates the lidar beam interaction with a wavy surface. The model has flexibility to produce a range of wavy surfaces and lidar parameters.

Finding #2 (W2): A wave tank was built and combined with a nadir-viewing lidar to observe the effects of wavy surfaces on the actual retrieval of range information from the backscattered lidar returns. The wave tank has flexibility to generate a range of wavelengths, from 0.12 to 0.7 meters, and amplitudes up to 4 centimeters. These waves can be simulated by the surface-wave model.

Finding #3 (W3): A lidar target morphometry test of a submerged brick using the wave tank at a specific wavelength and amplitude illustrated a spread in range values and cross-range values due to surface waves that blurred the edge, spread the top, and introduced a slight bias towards longer ranges. These effects were replicated by the wave model and identified that refraction through the wave slope (ratio of wave amplitude to wavelength) was impacting the cross-range

error the most, while the changing water path length due to observing in the crest and the valley of the wave caused the spread in range estimates. The range bias to longer range is attributed to refraction where a nadir viewing lidar will always increase in range when experiencing a slope other than flat. These results will vary depending on the wave representation and particularly on ratio of amplitude to wavelength.

Finding #4 (W4): The absolute estimate of error for all wave conditions is highly dependent on the lidar parameters and the water surface wave properties. The effects of refraction due to changing wave slope and time delay due to wave amplitude changes are clearly the dominant factors in producing range variability in range and cross range. The effects are observed in the data and captured by the wave-lidar model. Specific conditions will need to be known to fully quantify the effects but a conservative uncertainty of several centimeters (< 5 cm) in shallow waters (< 5 m) is the expected effect of surface waves on lidar target morphometry.

Finding #5 (W5): Through a series of wave tank experiments with varied wavelengths and amplitudes (22 different tests), the surface wave-lidar model was validated and can serve as a useful tool to evaluate lidar performance and help optimally design lidar parameters given an actual ocean wave spectrum.

Turbidity effects

Simulation results from the turbid water MCLST code are shown in Figures 11 and 12. The effect of turbidity on the laser beam is to spread the beam as it travels through water. For particles that are smaller than the wavelength of the laser light, the scattering phase function is very broad and scattering over large angles occurs causing the laser beam to spread out quickly through the water column. For particles which are bigger than the wavelength of the laser light, the scattering is predominantly forward, and the laser beam does not spread out as much. These results can be quantified by calculating the $1/e^2$ beam width of the laser light as it spreads downward through the water column.

This is done by fitting a 2-D Gaussian to the laser light at different water depths. As the depth increases, the light spreads out and the beam width increases due to the scattering in the water column. For smaller particles the beam spreads out quickly, at relatively small water depths, whereas for larger particles the beam spreads out slower for the same optical depth. This is shown in Figure 11 (for 10 nm particles) and Figure 12 (for 10 micron particles).

The addition of suspended particulates enhances extinction by scattering light in directions outside the field of view of the receiver. The efficiency of the scattering is dependent on the scattering regime as determined by the ratio of the particle circumference to the laser wavelength. A general description of scattering regimes can be provided by using the size parameter, $x=2\pi r/\lambda$, where r is the radius of the particle and λ is the wavelength of the laser light, i.e. 0.532 microns. Values of x below 0.2 refer to the Rayleigh scattering regime, between 0.2 and 10 refers to the Mie scattering regime, and greater than 10 the scattering becomes geometric

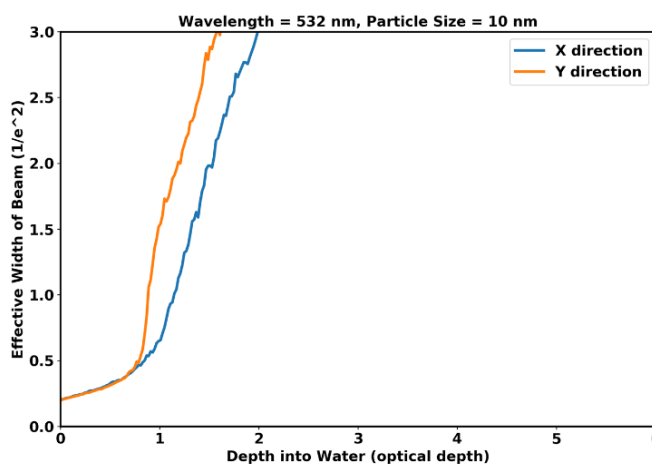


Figure 11. Lidar MCLST simulation of spreading of a lidar beam propagating through the water column with a uniform distribution of 10 nm spherical particles. The $1/e^2$ value of the Gaussian beam is tracked to indicate beam width.

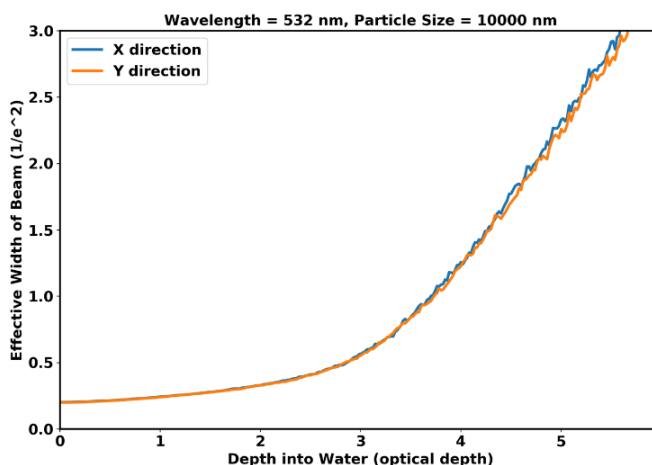


Figure 12. Lidar MCLST simulation of spreading of a lidar beam propagating through the water column with a uniform distribution of 10 micron particles. The $1/e^2$ value of the Gaussian beam is tracked to indicate beam width.

where more standard optical approaches, such as reflection, refraction and diffraction, can be applied [Bohren and Huffman, 1983].

The particles and their sizes used in the experiments shown in Table 1 cover the low end of the Mie regime for the three smallest particles to the Geometric regime for the larger particles. It

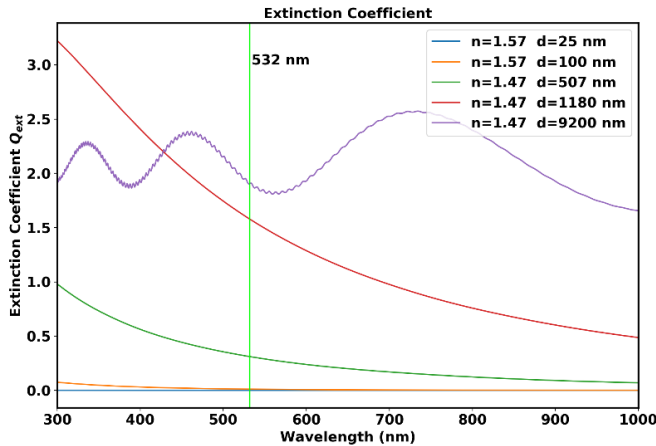


Figure 13. Lidar MCLST simulation of the extinction coefficient versus wavelength for different particle sizes .

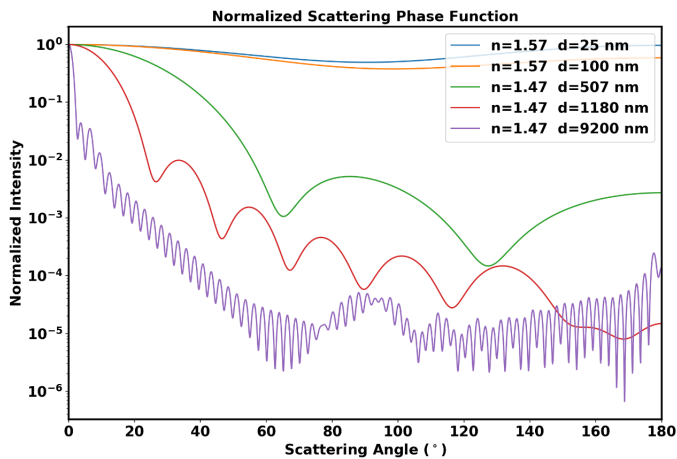


Figure 14. Lidar MCLST simulation of the normalized scattering phase function at 0.532 micron for different particle sizes used in the lab experiments.

turns out, this range in particle size can produce quite complex results in the extinction efficiency factor, Q_{ext} (the ratio of the energy scattered by the particle to the total energy in the incident beam intercepted by its geometric cross section). Figure 13 illustrates the Q_{ext} calculation using our Monte Carlo code. As the size parameter increases, the extinction efficiency factor approaches two due to diffraction of the optical wave front around the particle [Bohren and Huffman, 1983]. Furthermore, the angular distribution of the scattered radiation changes with changing size parameter, as shown in figure 14 as determined using the Monte Carlo code. As the size parameter increases from 1 to 100 the amount of radiation scattered in the forward direction increases appreciably relative to other directions and this forward scattering becomes narrower in angle. This preferential forward scattering will prove important in the interpretation of our lidar measurements.

Our experimental setup, operating as a lidar such that the two-way propagation is observed, includes

scattering light out of the path from particulates in the column and scattering light along the optical path in the forward direction as the particle size gets bigger. The lidar has a finite acceptance angle along the optical path and will be sensitive to the amount of forward scattering produced by the different scatterers as well as signal being scattered out of the path. Figure 15 shows the experimental results of the bottom signal's peak voltage reading for each particle size as the concentration is increased.

Mie Scattering (0.099, 0.507, and 1.18 micron particles, $x=1.18, 5.9, \text{ and } 13.9$): For this range of particle diameters a consistent trend can be seen in how the amplitude of the subsurface signal decreases with increasing particle concentration in a near-exponential manner. As seen in Figure 15, the small particles at 0.099 micron are less efficient in extinguishing the laser light than the other two particles of larger size for the same concentration. Figure 13 illustrates this point where the extinction scattering efficiency is smaller for smaller size parameter.

Geometric Scattering (9.2 micron particles, $x=108.7$): This regime has a more complex effect on lidar signals. The subsurface peak height does decrease as concentration increases, however, at a considerably slower rate than the smaller sized particles. Per Figure 8, a particle near 10 micron illuminated by laser light at 0.532 micron would have an extinction efficiency factor close to the smaller particles at 1.18 micron shown on the left graph of Figure 10. Although the efficiency factor may be similar, the angular distribution of scattered energy is significantly different with more of the energy directed in a narrow angle around the forward direction for the 10 micron size than the smaller sized particles. This would suggest that forward scattering by the larger particle size is helping the received signal more significantly than for the smaller particles. Thus, for larger particle sizes, the depth-performance of the lidar can be better than for the same concentration of smaller particles.

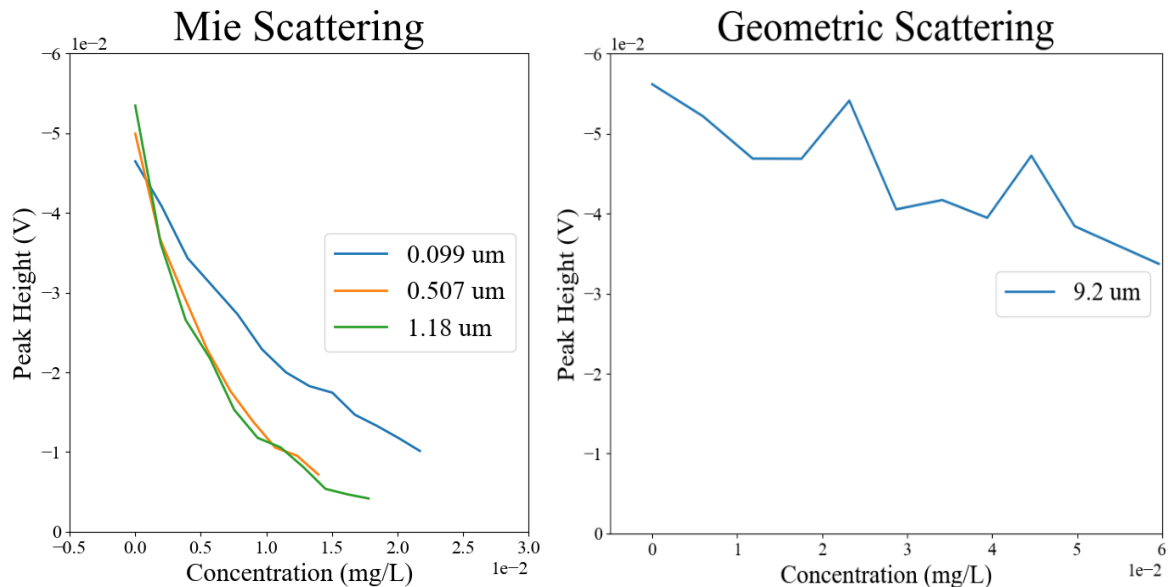


Figure 15. Bottom return signal voltage as a function of particle concentration for four discrete particle sizes. Sizes demonstrate the scattering regimes of weak and strong Mie scattering models and Geometric scattering. Note the horizontal range of the concentration for Geometric Scattering is extended to 0.060 mg/L.

These particulate scattering aspects will affect the ability to detect and classify objects, as a spreading beam will make small objects more difficult to discern and, for a given lidar receiver field-of-view, the number of photons received for detection will be reduced as many photons are scattered out of the path before returning to the lidar. However, greater forward scattering by

larger particulates helps the lidar depth performance by directing laser light within the field of view of the lidar.

The following is a summary of findings for turbidity effects (T#) on lidar performance.

Finding #6 (T1): A 3-D Monte Carlo model, the ASTRALiTe Monte Carlo Lidar Simulation Tool (MCLST), was developed to simulate laser light propagation through turbid water. Various lidar (beam size, divergence, polarization state, wavelength) and environmental (particulate size, particle density, index of refraction, absorption) variables can be adjusted in the model to fully explore the trade space of lidar parameters and environmental conditions. In the simulations photons from the lidar laser pulse are propagated through the water medium with uniformly distributed particulates of different particle size relative to the laser wavelength and each photon is tracked and counted to understand how the suspended particulate matter effects the laser light.

Finding #7 (T2): An experimental setup was built to validate the turbidity propagation model by mounting a stationary lidar system over a graduated cylinder and carefully controlling turbidity levels for specific particle sizes.

Finding #8 (T3): Experiments were conducted to match the model's conditions as closely as possible. A calibrated quantity of particles of uniform size and material are incrementally introduced into pure water and thoroughly mixed. Five different particle sizes were tested whose scattering regime ranged from weakly Mie scattering to Geometric scattering. For verification, the water turbidity was measured by a Nephelometer and recorded in Nephelometer Turbidity Units (NTUs).

Finding #9 (T4): The model simulations illustrated the adverse effect of beam spreading caused by the presence of suspended particulates. Using the size parameter as a reference, the spreading of the beam was greater for particles with size parameters closer to one (i.e., small particles - weakly Mie scattering) than for size parameters closer to one hundred (i.e., larger particles - Geometric scattering). These particulate scattering aspects will affect the ability to detect and classify objects, as a spreading beam will make small objects more difficult to discern and, for a given lidar receiver field-of-view, the number of photons received for detection will be reduced as many photons are scattered out of the path before returning to the lidar.

Finding #10 (T5): Congruently, the depth penetration was found to be size-parameter dependent with larger particles allowing for greater depth penetration than the smaller particles. The model showed through simulations of scattering phase function that the larger particles produced much more forward scattering keeping the photons in line with the lidar receiver field of view. This benefits detections to deeper waters than if the water column was populated with smaller particles of equal concentration.

Finding #11 (T6): Empirical results from the turbidity experimental setup confirmed the findings of the model with larger particles causing less light loss than the smaller particles for the same concentration. However, the outcomes can be less intuitive when the size parameter lies between weak and strong Mie scattering regimes. As simulated, the scattering efficiency and

scattering phase function are important parameters for determining laser light propagation and these depend on size parameter, particle index of refraction, particle concentrations and related optical properties. These properties will play an important role when working with particles in between weak and strong Mie scattering regimes (essentially between 0.01 and 1 micron particles when illuminated by 0.532 micron light).

Finding #12 (T7): The lidar’s optical detection of signals from underwater objects is favored by forward scattering of light caused by suspended particulates. These photons will remain in the lidar’s field of view and contribute to the population of photons scattered back to the lidar receiver by the object. Thus, particle size and particle concentration matter when considering the lidar depth performance. A Nephelometer measures extinction at a given wavelength at a 90-degree scattering angle and thus does not capture all aspects of how lidar is influenced by turbidity. However, the straight forward Nephelometer measurement serves as a common reference by which to relate lidar depth performance in different water bodies (as will be demonstrated in the outdoor experiments).

Outdoor results with both turbidity and waves

Outdoor experiments were carried out using a prototype drone-based, scanning lidar system in several different environments. One experiment was to evaluate the ability to observe an object of known dimension in shallow waters. This outdoor experiment flew the lidar system over a relatively clear water shoreline with two cinder blocks placed in shallow depths – see Figure 16. The cinder blocks were 8-inch wide x 8-inch tall x 16-inch long (20.32 cm x 20.32 x 40.64) with

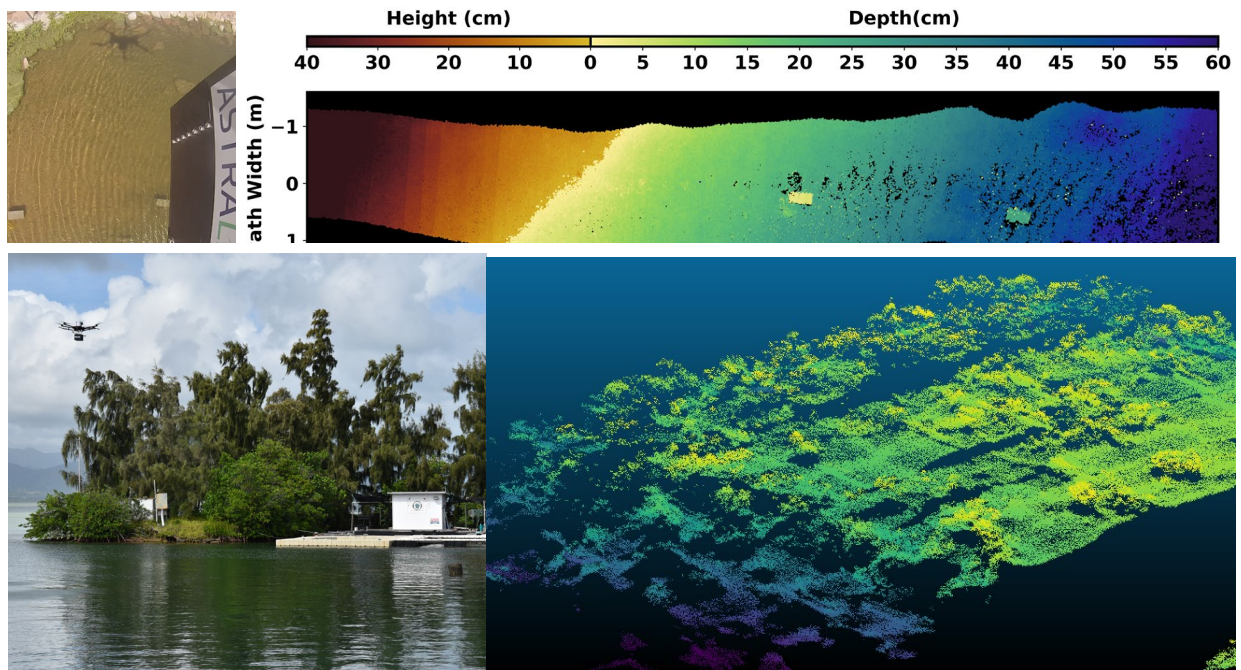


Figure 17. Drone-based scanning topo/bathy lidar flying over a lagoon with a coral bed (left). The resultant 3-D point cloud of the coral bed displaying great detail with the color variation indicating depth from water surface (yellow is about 1 meter depth and dark blue is about 4 meter depth)

one placed in the water about 16-cm deep and another in about 34-cm water depth. The blocks can be seen in the camera image taken from the drone platform shown in Figure 16. The lidar scanned side-to-side while the drone moved forward to produce an area covered with nearly 3000 pts/m² (an unprecedented level of detail). The color panel in Figure 16 is from one lidar pass using a color scale to indicate the derived depth of the water and height of the land. The lidar can seamlessly transition from land to water and can detect objects just below the water surface. Estimates of the cinder block dimensions were within a few centimeters and can easily be identified in the data point cloud.

Other outdoor experiments were focused on natural objects under the water. Figure 17 shows the drone-based, scanning topo/bathy lidar flying over a lagoon in Oahu, HI where a coral reef bed is submerged in waters that vary from 1 – 4 meters. The 3-D point cloud produced by the lidar measurements show in great detail the coral features of the submerged coral reef bed.

Turbidity Observations. Through a series of outdoor experiments with the drone-based lidar, a range of outdoor turbidity levels were experienced by the lidar system. Nephelometer measurements were collected for each outdoor experiment as a proxy by which to determine relative turbidity levels between water bodies. Figure 18 is a plot that summarizes the lidar’s depth performance for different levels of turbidity in nephelometer turbidity units (NTUs). This behavior meets expectations of a power law distribution in signal capability with penetration depth decreasing with increasing turbidity levels.

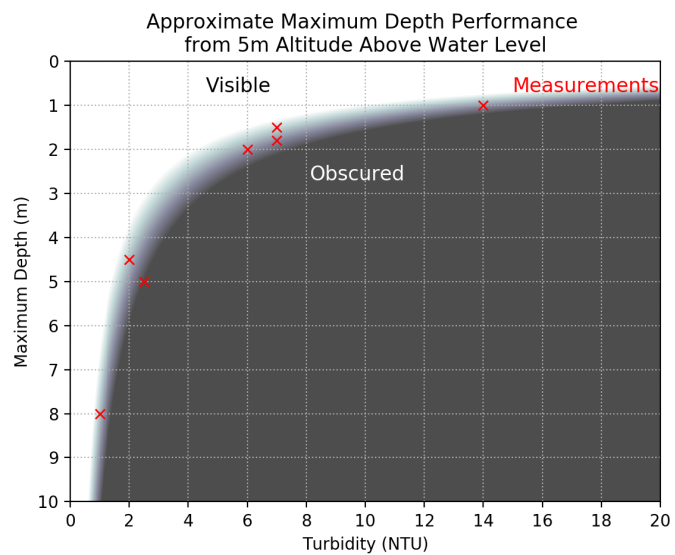


Figure 18. Lidar maximum depth performance in meters with turbidity levels in nephelometer turbidity units (NTU). The red X’s indicate actual depth measurements with measured NTUs from outside experiments.

Surface waves. A sample data set from an outdoor experiment under a variety of surface wave conditions is given in Figure 19 from a coastline region in Oahu, HI. The surface conditions were breaking waves at the coast and wind-driven waves away from the coastline. The picture in Figure 19 shows the water surface conditions. The lidar performed well by providing continuous 3-D mapping of underwater bathymetry at high-resolution (centimeter level) from land throughout most surface wave conditions. Breaking waves at the shore do introduce two effects which can limit the lidar’s ability to detect the bottom. One is surface foam that significantly scatters laser light and inhibits detection of the bottom surface. Another is the increased turbidity in the water column produced by breaking wave action. The surface foam can be overcome by its transient nature relative to the lidar while the turbidity is more extensive and persistent. The

detailed rock features are identified in the lidar data while being submerged several meters below

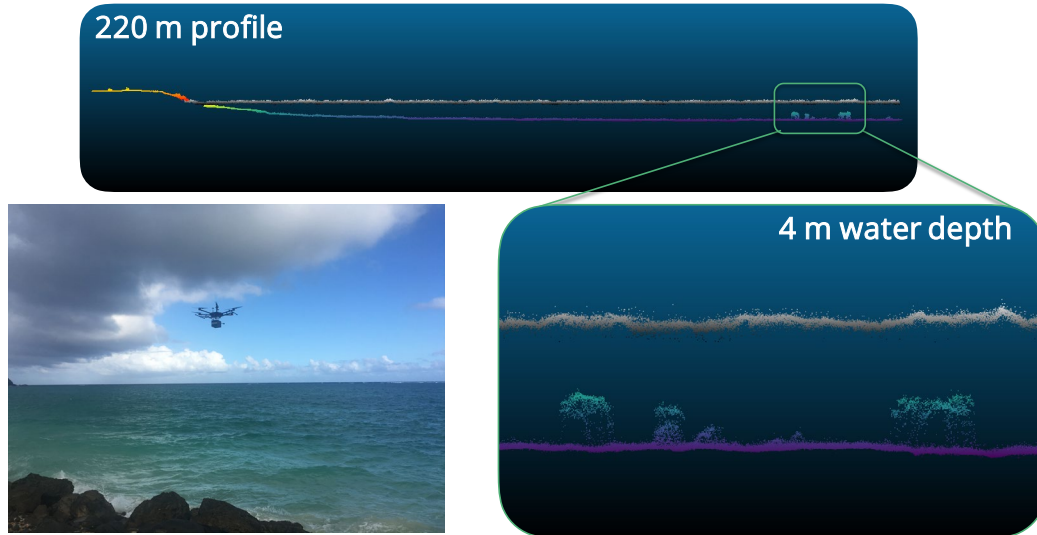


Figure 19. Outdoor experiments under wavy surface conditions off the coast of Oahu. The water surface conditions are shown in the lower left with the lidar mounted and flying on a drone above the surface. The top panel shows lidar measurements producing a 3-D mapping of land, the break wall, and the bay. The insert in the lower right provides detailed mapping of rocks submerged in about 4 meters of water depth along with surface details.

the wavy water surface. The data clearly indicates that wavy surfaces do not prevent detection of submerged objects in waters $< 5\text{m}$ (the targeted depth of the SERDP program), and that a high-resolution description of underwater objects within wavy surface conditions is highly achievable.

Outdoor experiments introduce other variables into the 3D mapping capability that increase the uncertainty in the measurement. A prominent variable is the uncertainty of the platform position and attitude. This uncertainty was addressed in these experiments by mounting a GPS receiver and an inertial measurement unit within the lidar payload and having a nearby base station for reference. Post processing of this data reduced significantly the platform position error to within typical values of 3-5 cm precision. The water wavy surface also introduced some uncertainty due to height and slope uncertainties, as discussed previously. Thus, the total uncertainty of the measurement (including lidar, platform, and surface variability) was determined to be predominantly $< 10\text{ cm}$. This error could be further reduced through improved GPS / IMU processing and developing a scheme to correct for uncertainty introduced by wavy surfaces.

The following is a summary of findings for outdoor observations (O#) on lidar performance.

Finding #13 (O1): Outdoor experiments with a prototype drone-based, scanning topographic / bathymetric lidar were carried out for different water bodies under different surface wave and turbidity conditions. Calibration targets were placed in the water and mapped by the lidar.

Finding #14 (O2): The outdoor experiments identified known targets in shallow water ($< 5\text{ m}$) with centimeter-level precision while also providing in great detail natural features such as individual coral within the coral reef bed.

Finding #15 (O3): The outdoor experiments experienced a range of turbidity levels in different water bodies. These levels were recorded by the same Nephelometer and an empirical curve of lidar depth to turbidity level was determined. As expected through modeling, the lidar depth performance followed a power law distribution with greater depth for decreasing NTU values.

Finding #16 (O4): The outdoor experiments experienced a range of wave conditions. A sample data set off the coast of Oahu, HI consisted of breaking shore waves and wind-driven waves further from shore. The lidar was able to map the sea floor in most of these wavy conditions and resolve detailed descriptions of 2 meter rocks in 4 meters of wavy surface water. The only limiting situation occurred when foam from breaking waves scattered laser light preventing bottom detections and increased turbidity caused by breaking wave action reduced light penetration.

Finding #17 (O5): The prototype, drone-based scanning topo/bathy lidar has proven the technique can work in waters expected for munitions response and, through the improved understanding of performance in wavy and turbid waters, a system could be optimally designed for such applications.

Conclusions and Implications for Future Research

The findings from our modeling, lab and outdoor experiments have established that our lidar technique is practicable for detecting and identifying munitions in waters less than 5 meters deep with a total uncertainty in both vertical and horizontal resolution of < 10 centimeters. This total error is a conservative empirical estimate based on the culmination of error introduced by the lidar (~1 cm), platform (~5 cm), and water conditions (~1-5 cm). We understand the impacts of surface conditions and suspended material within the column on the lidar performance to properly assess its ability under different environmental scenarios. We are confident that through future research we can transition these prototype findings to an operational, drone-based, topographic and bathymetric lidar system designed specifically for munitions response.

Future Research. The SEED grant has significantly advanced the lidar technique to a level of practical use for shallow water munitions response. However, there remains several areas of research needed to make the system operational. The research involves both environmental conditions and system design.

Although we have addressed the effects of surface waves and turbidity on the lidar performance, other environmental issues can impact lidar operations, such as sunlight and target reflectivity. Target reflectivity has a direct effect on lidar detectability by impacting the amount of light backscattered by the object. However, we employ polarization tactics in our lidar systems which also depend on the target's polarization scattering properties. This would be an area of research to explore and better understand how targets respond in different planes of polarization.

Sunlight degrades our system performance by lowering the signal to noise in detecting under water objects. Direct and diffuse sunlight scatter have different effects on the system and methods need to be pursued to diminish sunlight scatter from reaching the lidar detectors. This

would require research in the sunlight scatter expected and methods to employ in the lidar system to reduce this effect.

Another potential research area is to correct for wavy surface refraction by using the lidar to map the water's surface and fit a grid by which to correct the bottom returns based on the empirically determined wave properties.

Future research is also needed in system design for operations in such conditions as rain, humidity, heat, spray, and wind. The prototype has demonstrated capability but flight time, flight altitude, scanning coverage, measurement capability, and related design-to specifications are needed to be researched and mapped to the munitions response program's requirements. For example, research into reducing size, weight, and power would lead to longer flight times. Operating at higher altitudes would increase coverage but would require research into the design to improve performance as signal from bottom targets become weaker with greater distance from the water surface.

Integrating a camera system for data fusion between lidar and camera imagery would also be highly desirable and could enhance the measurement outcome.

Finally machine learning techniques on the retrieved lidar point cloud should be researched to automatically identify features such as water surface, water column, and underwater terrain or objects in the data and to produce real-time maps.

Benefits. The lidar-wave model and the turbidity model have proven to be very helpful in understanding observed behavior in underwater target morphometry for wavy and turbid conditions. In fact, these models will be instrumental in optimizing the lidar instrument design. Airborne lidar bathymetry parameters could be varied and tuned such that optimal performance is achieved for a given expectation of ocean conditions and environment.

The findings from this SEED grant are highly relevant to SERDP munitions response program, DoD, and science communities because this novel, above-water lidar technique could provide highly accurate ranging and mapping of submerged objects with centimeter-level precision, identify land-to-water transitions, provide accurate descriptions of bottom surface topography, object detection, object characterization, and precise water depth estimates, while eliminating risks associated with deploying traditional submerged sensors.

This lidar capability can be highly complementary to other SERDP techniques and can help provide a more complete description of the entire scene – particularly in shallow water. Like terrestrial lidar systems that determine indicators of prior munitions by detecting craters, aiming circles and other persistent surface features, the lidar technique could explore underwater bottom surface indicators of munitions activity. Providing such indicators may prove useful for quickly scanning large areas to identify likely munitions sites that will require further detailed investigation.

Furthermore, mobility modeling of munitions is dependent on environmental parameters, such as water depth and bottom and top surface morphologies, which the lidar can provide as model input. The lidar measurements can also be used as a tool for designing, planning and executing

surveys. An initial survey using the lidar technique can quickly provide data and insights for follow-on survey decision making, including reduction of risk to divers and other assets.

The results further address technology advancements by establishing a new technology with the ability to detect, range, and classify underwater objects with high vertical and horizontal resolution (< 10 cm) in shallow water (<5m) – without contacting the water. Relative to existing lidar systems, the resulting lidar provides unprecedented depth resolution and horizontal resolution for much improved hydrography, thus making survey results more useful. It also uses less expensive and less complex lidar components, which reduces the system cost and cost compared to other bathymetric lidar systems. The technology advancements have also led to reductions in size, weight, and power allowing for ASTRALiTe to develop the first drone-based, scanning topographic / bathymetric lidar.

Literature Cited

- Allouis, T., Bailly, J. S., Pastol, Y., & Le Roux, C. (2010). Comparison of LiDAR waveform processing methods for very shallow water bathymetry using Raman, near-infrared and green signals. *Earth Surface Processes and Landforms*, 35(6), 640-650.
- Bohren, C. F. and D. R. Huffman, Absorption and scattering of light by small particles, vol. 1. John Wiley & Sons, 1983.
- Brock, J. C., and S. J. Purkis (2009) The emerging role of lidar remote sensing in coastal research and resource management, *J. Coastal Res.*, 53, 1–5.
- Churnside, J. H., J. J. Wilson, and V. V. Tatarskii (2001) Airborne lidar for fisheries applications. *Opt. Eng.*, 40, 406–414.
- Guenther, G., and D. Maune (2007) Airborne lidar bathymetry. *Digital Elevation Model Technologies and Applications: The DEM users manual*. 2nd ed. ASPRS, 253–320.
- Guenther, G., M. Brooks, and P. LaRocque (2000a) New capabilities of the “SHOALS” airborne lidar bathymeter. *Remote Sens. Environ.*, 73, 247–255.
- Guenther, G., A. Cunningham, P. E. LaRocque, and D. J. Reid (2000b) Meeting the accuracy challenge in airborne lidar bathymetry. *Proc. Fourth European Association of Remote Sensing Laboratories (EARSeL) Workshop on Lidar Remote Sensing of Land and Sea, Dresden, Germany, European Association of Remote Sensing Laboratories*.
- Hasselmann, K. T. Barnett, E. Bouws, H. Carlson, D. Cartwright, K. Enke, J. Ewing, H. Gienapp, D. Hasselmann, P. Kruseman, et al., Measurements of wind-wave growth and swell decay during the joint north sea wave project (jonswap)," *Ergaenzungsheft 8-12*, 1973.
- Irish, J., and W. Lillycrop (1999) Scanning laser mapping of the coastal zone: The SHOALS system. *ISPRS J. Photogramm. Remote Sens.*, 54, 123–129.
- James, M. R., and Robson, S. (2012), Straightforward reconstruction of 3D surfaces and topography with a camera: Accuracy and geoscience application, *J. Geophys. Res.*, 117, F03017, doi:10.1029/2011JF002289.
- Jonasz M. and G. R. Fournier, *Light Scattering by Particles in Water: theoretical and experimental*, Academic Press, 2007.
- Mobley C. D., E. Boss, and C. Roesler, Ocean Optics Web Book, 2010.
- Mobley, C. D., Light and Water: radiative transfer in natural waters, Academic press, 1994.
- Pe’eri, S., and B. Long (2011) Lidar technology applied in coastal studies and management. *J. Coastal Res.*, 62, 1–5.
- Pe’eri, S., L. Morgan, W. Philpot, and A. Armstrong (2011) Land–water interface resolved from airborne lidar bathymetry (ALB) waveforms. *J. Coastal Res.*, 62, 75–85.